UNIVERSIDAD DE MÁLAGA

FACULTAD DE CIENCIAS

DEPARTAMENTO DE INGENIERÍA QUÍMICA

DOCTORAL PROGRAM

Química y Tecnologías Químicas, Materiales y Nanotecnología

Doctoral thesis

The preparation of activated carbon monoliths from biomass by-products for application in electrochemical and heterogeneous catalytic processes

Author: Paul O. I. Ibeh

Supervisors: Prof. Dr. D. Tomás Cordero Alcántara

Dr. Dña. Juana M.ª Rosas Martínez

Málaga, 2022

AUTOR: Paul Onyemaechi. I. Ibeh

https://orcid.org/0000-0002-3052-2446

EDITA: Publicaciones y Divulgación Científica. Universidad de Málaga

DECLARACIÓN DE AUTORÍA Y ORIGINALIDAD DE LA TESIS PRESENTADAPARA OBTENER EL TÍTULO DE DOCTOR

D./Dña Paul O.I Ibeh
Estudiante del programa de doctorado de la Universidad de Málaga, autor/a de la tesis,presentada para la obtención del título de doctor por la Universidad de Málaga, titulada: The preparation of activated carbon monoliths from biomass by-products for application in electrochemical and heterogeneous catalytic processes

Realizada bajo la tutorización de y dirección de D. Tomás Cordero Alcantara y Dña. Juana María Rosas Martínez

DECLARO QUE:

La tesis presentada es una obra original que no infringe los derechos de propiedad intelectual ni los derechos de propiedad industrial u otros, conforme al ordenamiento jurídico vigente (Real Decreto Legislativo 1/1996, de 12 de abril, por el que se aprueba el texto refundido de la Ley de Propiedad Intelectual, regularizando, aclarando y armonizando las disposiciones legales vigentes sobre la materia), modificado por la Ley 2/2019, de 1 de marzo.

Igualmente asumo, ante a la Universidad de Málaga y ante cualquier otra instancia, la responsabilidad que pudiera derivarse en caso de plagio de contenidos en la tesis presentada, conforme al ordenamiento jurídico vigente.

En Málaga, a 10 de Octubre de 2022

Fdo.: Doctorando	Fdo.:Tutor/a
Fdo.: Director/es de tesis	

llón de Gobierno. Campus El
Ejido.
29071
28 / 952 13 14 61 / 952 13 71 10
E-mail: doctorado@uma.es

D. Tomás Cordero Alcántara, Catedrático de Ingeniería Química de la Universidad de Málaga,

Dña. Juana M ª Rosas Martínez, Profesora Titular de Ingeniería Química de la Universidad de Málaga,

CERTIFICAN: Que el trabajo de investigación recogido en la presente Memoria ha sido realizado bajo su dirección, en el Departamento de Ingeniería Química de la Universidad de Málaga, por Don Paul O.I. Ibeh, y que reúne, a su juicio contenido científico suficiente y las condiciones necesarias para ser presentado y defendido ante el Tribunal correspondiente para optar el Grado de Doctor.

Málaga, Octubre 2022

Fdo.: Tomás Cordero Fdo.: Juana M.ª Rosas

INDEX

OBJECTIVES

The aim of this thesis is the preparation of binderless ACMs from lignin and olive stones. The first one derived from the pulp and paper industry and new biorefineries for bioethanol production (from lignocellulosic biomass); and the second one obtained from the olive industry. Kraft and Alcell® lignin, and olive stones, impregnated with H_3PO_4, are extruded, and subsequently activated. The obtaining of disks and monoliths with different amount of channels are also evaluated. In order to minimize the possible fusion and swelling of lignin during activation, different approaches have been tested. Furthermore, the electrochemical properties of the ACMs are analyzed.

On the other hand, this type of ACM were also evaluated as catalyst for the DME production. The activity and stability of these ACMs were analyzed for methanol dehydration reaction in air atmosphere. The influence of the presence of water on the dehydration of methanol

were also studied. A kinetic model was also proposed to reproduce the experimental results.

NOMENCLATURE

A_{BET}	BET Apparent Surface Area
A_{DR}	DR Surface Area
A_t	External Surface Area
ACMs	Activated Carbon Monoliths
AL	Alcell Lignin
BET	Brunauer, Emmett and Teller
C_g^{GCD}	GCD Specific Capacitance
C_v^{GCD}	GCD Volumetric Capacitance
CV	Cyclic Voltammetry
daf	dry ash free
DME	Dimethyl Ether
DR	Dubinin and Radushkevich
Ea	Activation Energy
ER	Eley-Rideal mechanism
EDLC	Electrochemical Double Layer Capacitor
GCD	Galvanostatic Charge-Discharge
IPA	Isopropyl Alcohol
K_{H2O}	Water Adsorption constant
K_{MeOH}	Methanol Adsorption constant
KL	Kraft Lignin
LH	Langmuir-Hinshelwood mechanism

MeOH	Methanol
MIP	Mercury intrusion porosimetry
NDIR	Non-Disperse Infrared
OS	Olive Stone
$\mathbf{P_{oIPA}}$	Isopropyl Alcohol as a function of inert atmosphere
$\mathbf{P_{MeOH}}$	Methanol as a function of atmosphere
PSD	Pore Size Distribution
SEM	Scanning Electron Microscopy
SO	Pseudo-Second Order
TPD	Temperature-Programmed Desorption
$\mathbf{V_{DR}}$	DR Pore Volume
$\mathbf{V_{mes}}$	Mesopore Volume
$\mathbf{V_t}$	Micropore Volume
$\mathbf{W/F_{oIPA}}$	Space time of isopropyl alcohol
$\mathbf{W/F_{MeOH}}$	Space time of methanol
XPS	X-ray Photoelectron Spectroscopy

List of Tables

List of Figures

Acknowledgements

I wish to show my profound gratitude and appreciation to Prof. Dr. Tomás Cordero Alcántara for his support and kindness throughout my studies in the PhD program at the University of Málaga (Spain), who doubled as the head of Chemical Engineering Department as well as my Project Director. His advice and encouragement were great tools that inspired and propelled me to this height. I would like to thank Prof. Dr. José Rodríguez-Mirasol for his contribution into my doctoral work as he was in constant touch with my Project Director to know the extent of the job carried out and was kind in his relationship with me.

My special appreciation is also directed to Dra. Juana Mª Rosas who was my Project Supervisor for her great motivation and interest in my PhD project, she was an inspiration and the brain behind the achievement of my Doctoral Thesis. Her patience and understanding was a source of hope and great determination to my success.

I would want to appreciate Dr Francisco Jose Garcia who is a colleague for his immense support and assistance throughout my PhD program. I would also want to give thanks to Dr Ramiro Rafael Ruiz Rosas who was always willing to assist when needed.

My special thanks to the Department of Chemical Engineering group called TERMA for their general support and especially the cooperation among themselves. They were very accommodating and were ready to assist in any capacity necessary.

I would like to thank in a special way my beloved wife and my entire family for their endless intercessory prayers for me, motivation and unlimited believe and optimism that I was going to come out successfully.

CHAPTER 1

INTRODUCTION

1. INTRODUCTION

Biomass is renewable organic material that comes from plants and animals. This includes crop residues, wood, crops and animal waste, among others. The estimated biomass production in the world is approximately 100 billion metric tons of carbon per year, about half in the ocean and half on land. Biomass is the most common form of renewable energy, widely used globally in most third world and developed countries, which can provide high-energy outputs to replace conventional fossil fuel energy sources. Biomass can be transformed into clean energy and/or fuels by a variety of technologies, ranging from conventional combustion process to advanced biofuels technology. Besides recovery of substantial energy, these technologies can lead to a substantial reduction in the overall biomass waste quantities requiring final disposal, which can be better managed for safe disposal in a controlled manner while meeting the pollution control standards [1, 2] specifically, biomass sources for energy include:

- ✓ Wood and wood processing wastes—firewood, wood pellets, and wood chips, black liquor from pulp and paper mills, etc.

- ✓ Agricultural crops and waste materials—corn, soybeans, sugar cane, switchgrass, woody plants and crop and food processing residues.
- ✓ Municipal solid waste-paper, cotton, and wool products, food, etc.
- ✓ Animal manure and human sewage.
- ✓ Forestry residues.
- ✓ Food processing waste.

Figure 1.1 summarized the different type of biomass sources. There are several commercial and industrial advantages and disadvantages of the use of biomass for energetic applications.

Advantages:

- Biomass is more widely available than fossil fuels.
- In most countries, growing biomass might provide a mechanism for financing the restoration of degraded land.
- Biomass energy can provide rural development and employment in developing countries, which can help to curb urban migration.
- Biomass as renewable energy can take something that is harming to the environment and convert it into something useful. For

example, garbage can be burned and converted into energy from biomass.

- Efficient use of wood waste resulting from wood can serve as an alternative source to fossil fuels for many homes.
- For sustainability, biomass production and use can lead to zero build-up of CO_2 in the atmosphere, because the CO_2 released during combustion is offset by the CO_2 extracted from the atmosphere during photosynthesis.
- Delocalized nature of biomass resources.
- For most developed countries, biomass for energy on excess farmland can provide livelihood for farmers [3].

Disadvantages:

The disadvantage of biomass during the production processes of biomass energy through combustion, pyrolysis, biogas fermentation, chemical transformation, etc., can be found as follows:

- It is expensive to carry out these processes because of the care for living things.
- More lands are needed because combustion products are required to be burned easily.

- Low energetic density.
- Environmental problems are created especially when the use of trees and tree product to power car is ineffective leading to more fuel consumption.

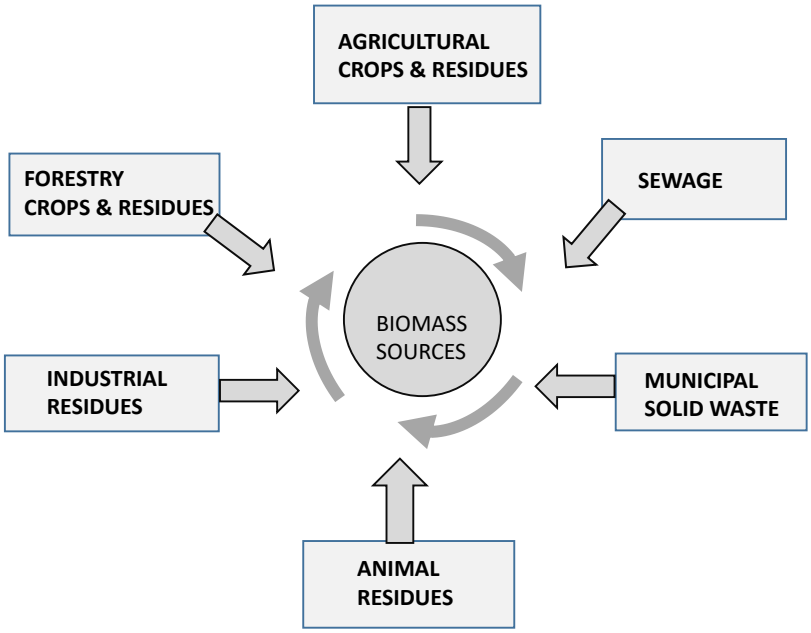

Figure 1.1 Biomass sources for energetic applications.

Biomass has been used as primary source of energy before fossil fuels and is still the dominant source of energy for the poorest people. In fact, the use of biomass fuels for transportation and for electricity generation is increasing in many developed countries as a means of avoiding carbon dioxide emissions from fossil fuel use. Biomass can be used for heating applications (such as wood stove) or electricity generation in a power

plant, just like burning coal. Specifically, the EU member states with a share of solid biomass used for electricity and heat production over 12% in 2018 were ranked. As can be seen in Table 1.1, Latvia was in the first place with a 31.9% share. Spain was ranked among the lagging countries with a solid biomass share of 5.1 %, very far from the target.

ble 1.1 Gross final energy consumption (GFEC) of solid biomass in EU countries [4].

Share of solid biomass in GFEC (2018)					
Leading countries (>12%)		**Intermediate group**		**Lagging countries (<6%)**	
31.9	Latvia	11.9	Bulgaria	5.6	Germany
31.1	Finland	11.7	Portugal	5.3	Greece
26.3	Sweden	10.3	Slovenia	**5.1**	**Spain**
26.2	Estonia	10.2	Czech R.	4.6	Belgium
22.1	Denmark	9.8	Hungary	4.1	UK
20.1	Lithuania	7.6	Poland	3.5	Cyprus
16.4	Croatia	6.7	France	2.7	Netherlands
15.0	Austria	6.5	Italy	2.2	Luxembourg
13.9	Romania	6.0	Slovakia	2.1	Ireland

However, the potential residual biomass resources in Spain are very high but are not yet exploited, mainly coming from forestry/farming activities and agricultural industries as can be seen in Table 1.2. In particular, the largest producers of residual biomass in Spain [5] are mainly derived from wood and furniture industry, followed by, in less extent, olive industry. The latter is the main contributor to residual biomass in Andalusia.

Table 1.2. Potential residual biomass in Spain in 2020 [5, 6].

Source		Potential biomass (tons/year)
Existing forest masses	Remains of felling	2984243
	Full tree use	15731116
Agricultural remains	Herbaceous	14434566
	Woody	16118220
Total		49268145

Therefore, among the different biomass waste available in Spain, this thesis is focused on the use of wood industry residues, in particular, lignin and olive stones.

Olive stones

Olive stone is a lignocellulosic material, with hemicellulose, cellulose and lignin as main components. The olive stone and seed are an important byproduct generated in the olive oil extraction and pitted table olive industries. It represents roughly 10% by weight of olive fruit and the amount of fixed and elemental carbon content within olive stone are around 16 and 47 wt%, respectively, which is considered as one of the highest values of carbon among various stone fruit [7].

In this sense, in an average season Spain produces around six million tons of olives, which are comprised of 15 percent pit. Between the seasoning and olive oil pressing industries, which pit most of the fruit they process, more than 450,000 tons of these seeds are amassed. Widespread olive stone use is directed towards its use as a solid fuel or its derivatives fuel as renewable source of energy [8]. However, many current studies aim to develop methods of recovering the lignocellulosic material or biomass in order to produce solid, liquid or gas biofuel.

Lignin

Specifically, lignin is one of the three basic components of wood and other lignocellulosics. Lignin is primarily a structural material to add

strength and rigidity to cell walls and constitutes between 15 and 40 wt% of the dry matter of woody plants. In addition, it can be considered as a three-dimensional amorphous aromatic polymer composed of a random network of phenylpropane groups. Three basic structures can be identified: p-hydroxyphenyl (H), guaiacyl (G) and syringyl (S); lignin can occur in a multiplicity of structures with different percentage values of H/G/S composition and by the types of bonds in which these units are connected. The total lignin amount of lignin present in the biosphere exceeds 300 billion tons and increases by approximately 7% every year.

Native lignin contains various types of functionalities. Common functional groups in lignin include methoxyl, phenolic, aliphatic, hydroxyl and other carbonyl groups in different percentages. Differences depends on: the plant family and species, part of the plant, age, and climate, and specific biomass treatment ("technical lignins").

One of the most important technical lignins is "**Kraft lignin**". This lignin is produced as byproduct of the paper/pulp industry and is the most dominant pulping process (black liquor). It constitutes approximately 630 kt (85%) of total lignin production [9].

This process involves treatment of wood chips with a hot mixture of water, sodium hydroxide (NaOH), and sodium sulfide (Na_2S), known as

white liquor that breaks the bonds that link lignin, hemicellulose, and cellulose [10]. The most common features of Kraft lignin achieved through the acid precipitation process of the black liquor is related to the small amount of sulfur (1–2% due to the use of Na_2S) and it is contaminated with carbohydrates from (hemi)cellulose [11].

The other type of technical lignin used in this thesis is "**Organosolv lignin**". This process is based on the hydrothermal treatment of biomass with a mixture of water, an organic solvent (methanol, ethanol, acetone) or a mixture and additional additives (often acids). The main characteristics of this lignin are its low molecular weight (1000–6000 g mol^{-1}) with relatively low dispersity, negligible content of sulfur, and low ash content (<1%). Compared to kraft lignin and lignosulfonate, it presents a more hydrophobic character.

In 2015, the worldwide production of lignin was 100 million tons, being most of the produced lignin consumed as a fuel in the pulp–paper industry to recover energy and chemical reactant, and only the 2% was actually being commercialized. The annual lignin production is expected to increase by 225 million tons per year in 2030 because of the increase of biofuel production [12, 13].

In fact, lignin is an ideal substitute for crude-oil-derived naphtha as a raw material for the synthesis of aromatic compounds, which ensures sustainability. Aromatic compounds serve as essential intermediates for the production of polymers, representing a healthy growth potential for aromatic lignin derivatives. The lignin market size from benzene-toluene-xylene (BTX) downstream potential surpassed USD 165 million in 2020 and is likely to grow at a CAGR of around 4% through 2027. In this sense, lignin serves as a renewable source of benzene that is conventionally produced from fossil fuels, offering ample growth potential [14].

Alternative uses of lignocellulosic waste

On the other hand, there is need for greater synergies between the circular economy and various biomass uses, particularly given the fact that biomass waste can be used for a range of products with higher added value than just energy. In this context, the conversion of lignocellulosic biomass waste into bio-based materials can be an interesting route for its valorization, and a further benefit for biomass waste-generating companies. Among the different possibilities, the preparation of activated carbon from these lignocellulosic biomass waste presents many

advantages, such as the great versatility and their exponentially increasing demand. Furthermore, it supposes an opportunity to obtain low-cost materials and to reduce environmental impacts.

The preparation of activated carbons from different lignocellulosic biomass waste such as olive stone, hemp residues, hazelnut shells, etc. has been extensively studied [15-19], but only a few papers analyzed the use of lignin as raw material for the production of activated carbons [20, 21]. This fact can be associated to the plastic and swelling behavior observed when lignin is pyrolyzed under N_2 atmosphere [22]. In spite of these technical problems, which have to be solved, isolation of lignin from pulping black liquors and the study of multiple applications for them has attracted considerable interest within a biorefinery context, overall due to the large amounts of lignin which could be generated in future wood-to-ethanol bio-refineries [23]. Therefore, the development of value-added lignin-based products, such as activated carbons, carbon fibers, carbon catalysts could be crucial to the economic success of the bio-ethanol production by this process.

In particular, ACs usually have a well-developed porous structure with a large internal surface area ranging from 500 to 2000 m^2/g, high thermal and chemical stability in both highly acidic and alkaline media and, in

addition, the chemistry of the carbon surface can be easily modulated. Furthermore, as aforementioned, they can be obtained from many diverse materials including different types of lignocellulosic waste. All these properties make them very suitable materials as adsorbent and catalyst supports [24-28].

There are different methods to prepare activated carbons. Among them, chemical activation is an enhanced approach in the preparation of activated carbon, which involves carbonization and activation. Chemical activation converts the raw precursor to a porous carbon material with elevated micropore and mesopore volume. The methodology consists of the impregnation of the raw material (for example: lignocellulosic waste), with certain chemical agents, which are thermally decomposed. The reagents most commonly used are zinc chloride, phosphoric acid or sulfuric acid.

Specifically, H_3PO_4 activation is a common method for the preparation of activated carbon due to its low energy consumption [29, 30], low pollution, and high yield. The raw material is usually mixed with different H_3PO_4 concentrations ranging from 30% to 60% in a certain impregnation ratio of 0.5 to 2.5, [31, 32] and then, activated at higher temperatures.

Phosphoric acid catalyzes the hydrolysis of the glycosidic linkages in hemicellulose and cellulose and it cleaves aryl ether bonds in lignin, obtaining many transformations that include dehydration, degradation and condensation. These reactions promote the release of H_2O, CO, CO_2 and CH_4 at low temperatures [33, 34].

In general, activation with phosphoric acid presents several advantages: (a) it occurs in a single or multiple thermal treatment process and leads to a high carbon yield, where the acid can be also economically recovered, (b) it is effective at relatively moderate temperatures, and (c) it results into materials with mixed porosity that widen the scope of its application.

Activated carbons are usually in form of powder; however, they can be present in different morphologies (powder, pellet, monolith, fiber). The application of the activated carbons and their cost will determine the most adequate morphology in each case.

Activated carbon monoliths preparation

The word "monolith" means "one stone" and refers to compact structures such as monoliths of the cylindrical and honeycomb types. The latter are

unit structures crossed lengthwise by parallel canals and constitute a new concept in the design of catalysts and adsorbents. These new structures offer low values drop to the passage of gases, facilitating the uniform flow of the same, excellent mechanical properties, a large surface area per unit weight or volume and they also behave like most adiabatic systems and reduce the constraints generated by the phenomenon of internal diffusion [35].

In addition, activated carbon monoliths (ACMs) offer several potential advantages over the granular activated carbons. For instance, they offer improved long-term stability due to reduced attrition, which in turn permits greater versatility in future equipment design. Furthermore, the monoliths present high thermal conductivity, as well as they are electrically conductive [36].

Many researchers have come up with different approaches to produce ACMs. Porous carbon monoliths can be prepared by different techniques and from different reagents:

❖ Template method: this method uses a selected material as a template, the reagent (carbon precursor) is imported into voids and reaction is initiated. Oftentimes, carbon monoliths prepared by this procedure reveals microporosity that comes from the carbon precursor,

and macro/mesoporosity that is formed upon the removal of either the solvent or the template, leading to a hierarchical porosity. At this way, it is able to prepare new type of material with controllable porosity. Template methods can be classified as hard and soft template method [37].

- Soft template method: this methodology uses surfactants as templates and the porous structure is formed by organic-organic self-assembly between the template and the carbon precursor. Finally, the ACM is obtained by the removal of the template. Fewer steps are needed compared to the hard templating route. This method also avoids the use of hazardous materials, thereby decreasing the negative impact on the environment However, the obtained ACM has limited pore size with low presence of large pores. This methodology can be difficult due to soft template is unstable.
- Hard template method: this method uses inorganic porous materials as template and the carbon precursor is filled into the voids by liquid phase impregnation or vapor deposition. Finally, the mixture is carbonized at high temperature to remove template. At this way, the ACM is the reverse of the inorganic template, showing high surface area, large pore volume and ordered

mesopores. Therefore, the pore size range is wider with this method, and easily tuned by changing the template, ensuring its applicability. In contrast, it requires several synthetic steps and they are costly due to the preparation of the inorganic colloid. Moreover, using chemicals such as hydrofluoric acid (highly dangerous) or sodium hydroxide solution (corrosive and environmentally unfriendly) for template removal is totally undesirable.

❖ Hydrothermal carbonization of biomass precursors in the presence of an activating agent, which acts as in-built template that prevents the adjacent cell walls from fusion/agglomeration during the carbonization and for the construction of porous carbon framework [38]. This methodology presents some drawbacks such as difficulty in scale-up, fairly long reaction time, and the nature of the batch processes involved [39].

❖ Preparation of ACM from natural monolithic biomaterials, such as pieces of wood, bone, etc., by physical activation [40] or chemical activation [41]. The obtained ACMs present poor mechanical properties and the availability of the precursors is much lower.

❖ Mold conforming under pressure of activated carbons or a carbon precursor followed by its carbonization. The main difficulty of this

methodology comes from the fact that compaction of powdered activated carbons does not lead to self-standing monoliths, but requires the use of a binder, which usually implies a reduction of pore sizes due to partial blocking, or in less extent in absence of any type of additive by applying a very high pressure [42-46].

Other alternative method is the extrusion of an impregnated material with different activating agents, such as H_3PO_4, KOH and $ZnCl_2$, until obtaining the adequate rheological conditions to be extruded [47-54].

Specifically, the preparation of binderless ACM from some kind of biomass waste has been already reported. For instance, ACM in form of disks were obtained from coconut shell and African palm by chemical activation with H_3PO_4 solutions [55-57]; ACM with six hexagonal parallel channels were prepared from African palm shells with H_3PO_4, $ZnCl_2$ and $CaCl_2$ solutions [58]; disks from coconut shells with zinc chloride [59]; honeycomb monoliths from orange peel with H_3PO_4, KOH, $ZnCl_2$, and water vapor (neither image was reported in this case) [60]; and pellets from olive stones with H_3PO_4 [61]. These previous works used the activating agent as a binder to proceed with the extrusion, followed by the activation of the ACM. Other methods proposed in the literature prepared disks from fibres of oil palm empty fruit bunches and

rubber wood sawdust by direct carbonization, compression and further activation with CO_2, respectively [62]; and disks from olive stones with KOH activation, followed by compression in the presence of polyvinylalcohol as binder [63].

1.1 Catalytic applications of ACM

Monolithic configurations usually present large geometric surface area, which results in a low-pressure drop when there are high flow rates, making them very useful materials to be used as adsorbents and supports for catalysts in environmental applications. Specifically, monolith conformation presents diverse advantages in catalytic applications, due to the fact that they offer better mass transfer, low pressure drop, thermal stability, and good mechanical strength [64]. In this sense, the use of carbon materials as catalysts and/or catalyst supports is receiving great attention [65]. Within this context, the use of this type of materials for the production of dimethyl ether (DME) is not extensively studied.

DME production

DME is the simplest aliphatic ether (CH_3-O-CH_3). DME is a chemically stable colorless, non-toxic, non-carcinogenic, and environmentally

friendly compound presenting a characteristic odor. At standard conditions, it is a gas, but can be easily liquified, obtaining properties similar to liquified petroleum gases (LPG). The importance of DME lies in the fact that it is recognized as a clean diesel substitute, due to its high cetane number (CN= 55-60), being environmental friendly with zero ozone depletion potential and a key intermediate for other important chemicals, such as olefins.

DME can be produced by two alternative processes: (a) a two-step process (namely indirect process), which consists of a first stage of methanol production from synthesis gas, followed by a its dehydration on a solid acid catalyst, (b) a direct process, where synthesis gas produces directly DME using a bifunctional catalysts.

This thesis is focused on the second step in the indirect DME synthesis. This formation is governed by the following equilibrium reaction:

$$2CH_3OH \leftrightarrow CH_3OCH_3 + H_2O \qquad \Delta H_r^o = -21.3\ kJ/mol$$

This reaction takes place in the temperature range of 250-400 ºC, at atmospheric pressure, in a fixed bed reactor, with solid acid catalysts. The most studied catalysts are zeolite materials, γ-Al_2O_3, and acid modified γ-Al_2O_3. However, most of these solid acid catalysts suffer from fast deactivation due to coke deposition over strong acid sites, and, in addition, their catalytic activities are usually negatively influenced by

the presence of water [66,67]. Therefore, the look for alternative catalysts with improved levels of performance is considered to be an important challenge.

In this sense, only few works analyzed the use of activated carbons for methanol dehydration due to their lowest surface acidity. This acidity can be eventually increased by different methods [68–70], but no outstanding results were obtained due to the low stability of the acidic surface sites produced. In this regard, our research group has reported the preparation and characterization of activated carbons from different lignocellulosic biomass waste by chemical activation with phosphoric acid at specific preparation conditions [71, 72]. This preparation method provides activated carbons with a high development of the porosity, relatively high oxidation resistance [73, 74], and a relatively large presence of low to moderate acid strength sites [75, 76]. These activated carbons were used as catalyst supports [72, 77, 78], and even directly as acid catalysts for alcohols dehydration reaction [75, 79–81], including methanol dehydration. In the absence of oxygen, this type of catalyst showed a gradual deactivation due to coke deposition. However, high stability and selectivity to DME was reached under the air atmosphere, due to the fact that oxygen prevented the acid carbon catalyst from coke

deposition, without gasification of the carbon catalyst was noticeable [76].

1.2 Electrochemical applications of ACM

A supercapacitor is a type of capacitor that can store a large amount of energy, typically 10 to 100 times more energy per unit mass or volume compared to electrolytic capacitors. It is preferred to batteries owing to its faster and simpler charging, and faster delivery of charge, long cycle life, etc. A supercapacitor is also known as ultracapacitor or double-layer electrolytic capacitor.

They are made of different porous materials such as metallic and carbon-based porous materials immersed in an electrolyte. Most supercapacitors are categorized into two kinds: pseudocapacitive and Electrochemical Double Layer Capacitor (EDLC) [82].

When voltage is applied to a supercapacitor, ions in the electrolyte solution diffuse into the pores of the electrode of opposite charge. Charge accumulates at the interface between the electrodes and the electrolyte, forming two charged layers (double layer) with a small separation distance, which is the distance between the electrode surfaces to the center of the ion layer. Capacitance (c) value is proportional to the

surface area (a) and is the reciprocal of the distance (d) between the two layers (c=a/d) [83]. Figure 1.2 shows a schematic representation of a supercapacitor.

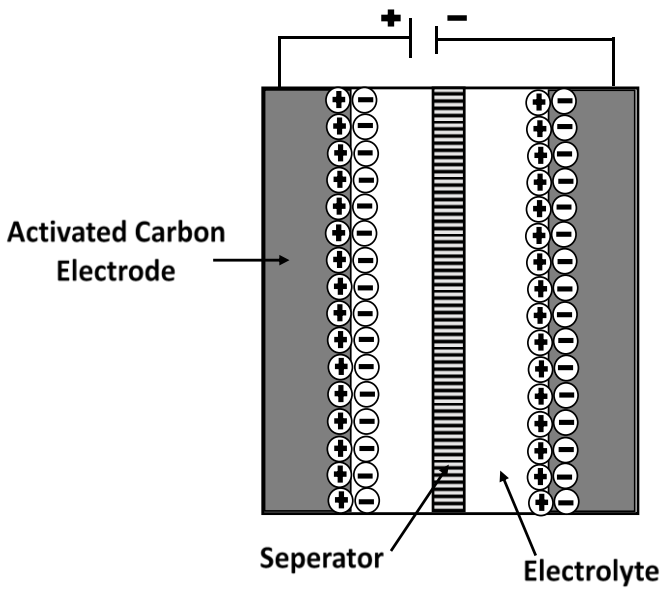

Figure 1.2. Supercapacitor -EDLC

ACMs have also shown promising results as electrodes for supercapacitors, due to their three-dimensional framework of interconnected carbon particles that lead to high electrical conductivity and good accessibility of the electrolyte. The contact between adjacent particles in all-carbon monoliths is much better than that observed in pellets made from compaction under pressure of a powdered carbon and an inert polymer [84-85].

Another advantage of the carbon monoliths is their hierarchical porous structure, derived from the connectivity of macro (>50 nm), meso (2-50 nm) and micropores (< 2 nm), which can work as reservoirs and feeders of the electrolyte and provide a large double layer as a result of their large specific surface area. All the carbon present in the monoliths can contribute to the capacitance. Furthermore, the bimodal pore size distribution of ACMs presents the advantage that small pores offer high effective surface area for electrochemical reactions, whereas large pores facilitate electrolyte ingress throughout the structure. In particular, the importance of these macropores is increased when employing an aqueous electrolyte because of the hydrophobic surface of carbon [86]. Additionally, they present relatively higher energy density than powder activated carbons.

In addition, the use of ACMs avoids the use of additives, such as binder and conductive agents. In this sense, the electrodes processed as compacted pellets of powdered carbon and polymeric binder can present isolated portions of the carbon, which are embedded in the binder and do not contribute to the capacitance.

The main drawback of the activated carbon monoliths is their low density, typically below 0.4 g cm^{-3}, that leads to low volumetric

capacitances, usually below 100 $F \cdot cm^{-3}$ in aqueous electrolyte and below 50 $F \cdot cm^{-3}$ in organic electrolytes [87].

1.3 References

[1] Bergman P. C. A, Kiel J. H. A. Torrefaction for biomass upgrading. European Biomass Conference & Exhibition, Paris 2005. https://www.researchgate.net/publication/228699171_Torrefaction_for_biomass_upgrading.

[2] Pirraglia A, Gonzalez R, Saloni D, Denig J. Technical and economic assessment for the production of torrefied lignocellulosic biomass pellets in the US. Energy Conversion and Management, 2013, 66, 153-164.

[3] Johansson T.B, Kelly H, Reddy K.N. A, Williams R. H. Renewable Energy: sources for fuels and electricity, 1993. https://www.cambridge.org/core/journals/environmental-conservation/article/abs/renewable-energy-sources-for-fuel-and-electricity.

[4] European Commission. National Renewable Energy Action Plans (NREAP's) EC, 2018. https://www.science.com/science/article/pii/S0960148120317900

[5] Menéndez J. A, Fernández-Tresguerres L. G, Villanueva S. F, Durán M, Montes-Morán M. A, Arenillas A. Report on the availability of Biomass Sources in Spain: vineyards and olive groves, 2018.

https://digital.csic.es/bitstream/10261/158364/1/Availability%20of%20Biomass%20Sources%20in%20Spain.pdf.

[6] Pélets de biomasa en España. Bioplat, 2012.

https://www.pfcyl.es/sites/default/files/biblioteca/documentos/presentacion_del_informe_pelets_de_biomasa_en_espana.pdf.

[7] González J.F, González-García C.M, Ramiro A. Combustion optimisation of biomass residue pellets for domestic heating with a mural boiler. Biomass Bioenergy, 2004, 27,145–154. DOI:10.1016/J.BIOMBIOE.2004.01.004

[8] Rodríguez G, Lama A, Rodríguez R, Jiménez A, Guillén R, Fernández-Bolaños J. Olive Stone an attractive source of bioactive and valuable compounds. Bioresource Technology, 2008, 99 (13) 5261-5269.

[9] Haq I, Mazumder P, Kalamdhad A. S. Recent advances in removal of lignin from paper industry wastewater and its industrial applications-A review. Bioresource Technology, 2020, 312, 123636

[10] Chemistry. Kraft process.
https://handwiki.org/wiki/Chemistry:Kraft_process

[11] Lange H, Bartzoka E. D, Crestini C. 11. Lignin biorefinery: structure, pretreatment and use. Biorefineries. 2015, 257-282. https://doi.org/10.1515/9783110331585-015.

[12] Hodásová L, Jablonský M, Škulcová A, Ház A. S. Lignin, potential products and their market value. Wood Research, 2015, 60 (6), 973-986. http://www.centrumdp.sk/wr/201506/13.pdf

[13] Bajwa D, Pourhashem G, Ullah A, Bajwa S. A concise review of current lignin production, applications, products and their environmental impact. Industrial Crops and Products, 2019, 139, 111526.

[14] Ahuja K, Bayas S. Lignin Market Size, By Product (Kraft Lignin, Lignosulphonates, Low Purity Lignin), By Application (Aromatics, Macromolecules), Industry Analysis Report, Regional Outlook, Lignin Downstream Potential (Vanillin, Carbon Fiber, Phenol, BTX), Application Potential, Price Trends, Competitive Market Share & Forecast 2021 – 2027, 2020. Global Insight Market. https://www.gminsights.com/industry-analysis/lignin-market, accessed 13th March 2022.

[15] Molina-Sabio M, Rodríguez-Reinoso F , Caturla F , Sellés M.J. Porosity in granular carbons activated with phosphoric acid. Carbon 1995, 33, 1105–13.

[16] Rosas J.M , Bedia J , Rodríguez-Mirasol J , Cordero T. Hemp-derived activated carbon fibers by chemical activation with phosphoric acid. Fuel 2009, 88, 19–26.

[17] Rodríguez G, Lama A , Rodríguez R , Jiménez A , Guillén R , Fernández-Bolaños J. Olive stone an attractive source of bioactive and valuable compounds. Biore- sour Technol 2008, 99, 5261–9.

[18] Fan HT, Shi L.Q, Shen H , Chen X , Xie K.P. Equilibrium, isotherm, kinetic and thermodynamic studies for removal of tetracycline antibiotics by adsorption onto hazelnut shell derived activated carbons from aqueous media. RSC Adv., 2016, 6, 109983–91.

[19] You N, Li J.Y, Fan H.T, Shen H. In-situ sampling of nitrophenols in industrial wastewaters using diffusive gradients in thin films based on lignocellulose-derived activated carbons. J Adv. Res., 2019, 15, 77–86.

[20] Rosas J.M, Berenguer R, Romero M.J.V, Rodríguez-Mirasol J, Cordero T. Preparation of different carbon materials by thermochemical conversion of lignin. J Front Mater 2014, 1, 29.

[21] Rodríguez J.J., Cordero T., Rodríguez-Mirasol J. Carbon Materials from Lignin and Their Applications. Production of Biofuels

and Chemicals from Lignin. Biofuels and Biorefineries, 2016, 217-262. https://doi.org/10.1007/978-981-10-1965-4_8

[22] Jin W, Shen D, Liu Q, Xiao R. Evaluation of the co-pyrolysis of lignin with plastic polymers by TG-FTIR and Py-GC/MS. Polymer Degradation and Stability, 2016, 133, 65-74.

[23] Gutierrez M.C, Rosas J.M, Rodríguez-Cano M.A, Luque I, Rodriguez-Miraso J, Cordero T. Strategic situation, design and simulation of a biorefinery in Andalusia. Energy Convers Manag 2019, 182, 201–14.

[24] Rodríguez-Mirasol J, Bedia J, Cordero T, Rodríguez J.J. Influence of water vapor on the adsorption of VOCs on lignin-based activated carbons. *Sep. Sci. Technol.* 2005, 40, 3113–3135.

[25] Ioannidou O, Zabaniotou A. Agricultural residues as precursors for activated carbon production. *Sustain. Energy Rev.*, 2007, 11, 1966–2005.

[26] Rosas J. M, Bedia J, Rodríguez-Mirasol J, Cordero T. Hemp-derived activated carbon fibers by chemical activation with phosphoric acid. Fuel, 2009, 88, 19–26.

[27] Rosas J. M, Bedia J, Rodríguez-Mirasol J, Cordero T. On the preparation and characterization of chars and activated carbons from orange skin. *Fuel Proc. Technol.* 2010, 91, 1345–1354.

[28] Radovic L. R, Rodríguez-Reinoso F. *Chemistry and Physics of Carbon*, 1997, 25, 243–358.

[29] Chen D. Z, Zhang J. X, Chen J. M. Adsorption of methyl tert-butyl ether using granular activated carbon: Equilibrium and kinetic analysis Int. J. Environ. Sci. Tech. 2010, 7 (2) 235-242.

[30] Arvelakis S, Crocker C, Folkedahl B, Pavlish J, Spliethoff H. Activated carbon from biomass for mercury capture: Effect of the leaching pretreatment on the capture efficiency, Energy Fuels. 2020, 24(3) 4445-4453.

[31] Cui J, Cui L, Cheng F, Liu L, Sun H, Li S. A green route for preparation of low surface area SiO_2 microspheres from wheat straw ash with activated carbon and NPK compound fertilizer as by-products, *RSC Advances*, 2015, 5 (98), 80238-80244.

[32] Zhu N, Yan T, Qiao J, Cao H. Synthesis of manganese chloride activated carbon deriving from wheat straw and its adsorption mechanism for arsenic and chromium, International Journal of Environmental Analytical Chemistry, 2016, 3(1), 2380-2391.

[33] Jagtoyen M, Derbyshire F. Activated carbons from yellow poplar and white oak by H_3PO_4 activation. Carbon. 1998, 36, 1085-97.

[34] Rodríguez-Mirasol J, Cordero T, Rodríguez J. J. Preparation and characterization of activated carbons from eucalyptus kraft lignin. Carbon.1993, 1, 87–95.

[35] Yates M, Blanco J, Avila P, Martin M. P. Honeycomb monoliths of activated carbons for effluent gas purification. Microporous and Mesoporous, 2000, 37 (1-2), 201-208.

[36] Chinn M, Hindmarsh C, Keel H.E. Electrical Swing Regenerable Filtration Using Carbon Fibre Composites and Carbon Monoliths, Engineering, 2004. https://www.hsdl.org/?view&did=453227.

[37] Lei L, Zhongyong Y. Soft Template Synthesis of Ordered Mesoporous Carbon Materials. Progress in Chemistry 2014, 26 (05), 756-771.

[38] Kryssanova K, Krylova A, Zaichenko V.M. Application of Hydrothermal carbonization to improve the energy property of peat. Solid Fuel Chemistry, 2021, 55(2), 123-128. DOI: 10.3103/S0361521921020026

[39] Raghu Kc, Babu I, Alatalo S, Föhr J, Ranta T, Tiihonen I. Hydrothermal Carbonization of Deciduous Biomass (Alnus incana) and

Pelletization Prospects. Journal of Sustainable Bioenergy Systems, 2017, 7, 138-148. Doi: 10.4236/jsbs.2017.73010.

[40] Iwantona E. T, Manik S, Taslim R, Dahlan D, Deraman M. Preparation of activated carbon monolith electrodes from sugarcane Bagasse by physical and physical-chemical activation process for supercapacitor application. Advanced Material Research, 2014, 896, 179-182.

[41] Gonzalez-Serrano E, Cordero T, Rodriguez-Mirasol J, Cotoruelo L, Rodriguez J.J. Removal of Water Pollutants with Activated Carbons Prepared from H_3PO_4 Activation of Lignin from Kraft Black Liquors. Water Res., 2004, *38*, 3043.

[42] Lozano-Castelló D, Cazorla-Amorós D, Linares-Solano A, Quinn DF. Activated carbon monoliths for methane storage: influence of binder. Carbon 2002, 40, 2817–25.

[43] Lim J.W, Choi Y, Yoon H.S, Park Y.K, Yim J.H, Jeon J.K. Extrusion of honeycomb monoliths employed with activated carbon-LDPE hybrid materials. J Ind Eng Chem 2010, 16, 51–6.

[44] Liu L, Liu Z, Yang J, Huang Z, Liu P. Effect of preparation conditions on the properties of a coal-derived activated carbon honeycomb monolith. Carbon 2007, 45, 2836–42.

[45] Machnikowski J , Kierzek K , Lis K , Machnikowska H , Czepirski L . Tailoring porosity development in monolithic adsorbents made of KOH-activated pitch coke and furfuryl alcohol binder for methane storage. Energy Fuels 2010, 24, 3410–14.

[46] Jorda-Beneyto M, Lozano-Castelló D, Suárez-García F, Cazorla-Amorós D, Linares-Solano A. Advanced activated carbon monoliths and activated carbons for hydrogen storage. Microporous Mesoporous Mater, 2008, 112,235–42.

[47] Garcia-Bordeje E, Kapteijn F, Moulijn J.A. Preparation and characterization of carbon-coated monoliths for catalyst supports. Carbon 2002, 40, 1079–88.

[48] Ozaki J, Endo N, Ohizumi W, Igarashi K, Nakahara M, Oya A, Yoshida S, Iizuka T. Novel preparation method for the production of mesoporous carbon fiber from a polymer blend. Carbon, 1997, 35, 1031-3.

[49] Lazar F.S, Chaieb T, Pallier S, Veyre L, Philippe R, Meille V. Direct coating of carbon-supported catalysts on monoliths and foams -singular behaviour of Pd/MWCNT. Appl. Catal. A Gen., 2015, 508, 45–51.

[50] Lam E, Luong J.H.T. Carbon materials as catalyst supports and catalysts in the transformation of biomass to fuels and chemicals. ACS Catal. 2014, 4, 3393–410.

[51] Hulicova D, Oya A. The polymer blend technique as a method for designing fine carbon materials. Carbon 2003, 41, 1443–50.

[52] Vergunst T, Linders M.J.G, Kapteijn F, Moulijn J.A. Carbon-based monolithic structures. Catal Rev Sci Eng 2001, 43, 291–314.

[53] Molina-Sabio M, Almansa C, Rodríguez-Reinoso F. Phosphoric acid activated carbon disks for methane adsorption. Carbon 2003, 41, 2113–19.

[54] Pérez-Cadenas A.F, Kapteijn F, Moulijn J.A, Maldonado-Hódar F.J. Pd and Pt cat- alysts supported on carbon-coated monoliths for low-temperature combustion of xylenes. Carbon 2006, 44, 2463–8.

[55] Vargas D.P, Giraldo L, Silvestre-Albero J, Moreno-Piraján J.C. CO2 adsorption on binderless activated carbon monoliths. Adsorption 2011, 17, 497–504.

[56] Vargas D.D.P, Giraldo G.L, Moreno P.J.C. Enthalpic characterisation of activated carbon monoliths obtained from lignocellulosic materials. J Thermal Anal Calorim 2013,111, 1067–72.

[57] de Oliveira J.C.A, Rios R.B, López R.H, Zgrablic G. Monte Carlo simulation strate- gies for predicting CO2 /CH4 adsorption onto activated carbons from pure gas isotherms. Adsorpt Sci Technol 2011, 29, 651–61.

[58] Vargas D.P, Giraldo L, Moreno-Piraján J.C. CO2 adsorption on activated carbon honeycomb-monoliths: a comparison of Langmuir and Tóth models. Int J Mol Sci 2012, 13, 8388–97.

[59] García-Blanco AA , Alexandre de Oliveira JC , López R , Moreno-Piraján JC , Gi- raldo L , Zgrablich G , Sapag K . A study of the pore size distribution for activated carbon monoliths and their relationship with the storage of methane and hy- drogen. Colloids Surf A Physicochem Eng Asp 2010,357, 74–83.

[60] Giraldo L, Bastidas-Barranco M, Moreno-Pirajan J.C. Preparation of carbon monoliths from Orange peel for NOx Retention. Oriental J Chem 2014, 30, 1517–28.

[61] Djeridi W, Ouederni A, Wiersum AD, Llewellyn PL, El Mir L. High pressure methane adsorption on microporous carbon monoliths prepared by olives stones. Mater Lett 2013, 99, 184–7.

[62] Taer E, Deraman M, Taslim R, Iwantono. Preparation of binderless activated carbon monolith from pre-carbonization rubber wood sawdust

by controlling of carbonization and activation condition. AIP Conf Proc 2013, 33, 1554.

[63] Pérez RU, Marín FC, Jiménez DF, Castilla C.M. Granular and monolithic activated carbons from KOH-activation of olive stones. Microporous Mesoporous Mater 2006, 92, 64–70.

[64] Govender S, Friedrich H. Monoliths: A Review of the Basics, Preparation Methods and Their Relevance to Oxidation. *Catalysts* 2017, *7*, 62.

[65] Rodríguez-reinoso F. The role of carbon materials in heterogeneous catalysis. *Carbon* **1998**, *36*, 159–175.

[66] Pérez-Uriarte P, Ateka A, Gayubo A.G, Cordero-Lanzac T, Aguayo A.T, Bilbao J. Deactivation kinetics for the conversion of dimethyl ether to olefins over a HZSM-5 zeolite catalyst. *Chem. Eng. J.* **2017**, *311*, 367–377.

[67] Aguayo T, Gayubo A.G, Vivanco R, Olazar M, Bilbao J. Role of acidity and microporous structure in alternative catalysts for the transformation of methanol into olefins. *Appl. Catal. A Gen.* **2005**, *283*, 197–207.

[68] Zawadzki J, Azambre B, Heintz O, Krztoń A, Weber J. IR study of the adsorption and decomposition of methanol on carbon surfaces and carbon-supported catalysts. *Carbon* **2000**, *38*, 509–515.

[69] Jasiñska J, Krzyžyñska B, Kozłowski M. Influence of activated carbon modifications on their catalytic activity in methanol and ethanol conversion reactions. *Cent. Eur. J. Chem.* **2011**, *9*, 925–931.

[70] Moreno-Castilla C, Carrasco-Marín F, Parejo-Pérez C, López-Ramón M. Dehydration of methanol to dimethyl ether catalyzed by oxidized activated carbons with varying surface acidic character. *Carbon* **2001**, *39*, 869–875. *Materials* **2019**, *12*, 2394 13 of 14

[71] Rosas J.M, Bedia J, Rodríguez-Mirasol J, Cordero T. Preparation of hemp-derived activated carbon monoliths. Adsorption of water vapor. *Ind. Eng. Chem. Res.* **2008**, *47*, 1288–1296.

[72] Bedia J, Rosas J.M, Rodríguez-Mirasol, J, Cordero T. Pd supported on mesoporous activated carbons with high oxidation resistance as catalysts for toluene oxidation. *Appl. Catal. B Environ.* **2010**, *94*, 8–18.

[73] Rosas J.M, Bedia J, Rodríguez-Mirasol J, Cordero T. HEMP-derived activated carbon fibers by chemical activation with phosphoric acid. *Fuel* **2009**, *88*, 19–26.

[74] Rosas J.M, Ruiz-Rosas R, Rodríguez-Mirasol J, Cordero T. Kinetic study of the oxidation resistance of phosphorus-containing activated carbons. *Carbon* **2012**, *50*, 1523–1537.

[75] Bedia J, Rosas J.M, Márquez J, Rodríguez-Mirasol J, Cordero T. Preparation and characterization of carbon based acid catalysts for the dehydration of 2-propanol. *Carbon* **2009**, *47*, 286–294.

[76] Valero-Romero M.J, Calvo-Muñoz E.M, Ruiz-Rosas R, Rodríguez-Mirasol J, Cordero T. Phosphorus-Containing Mesoporous Carbon Acid Catalyst for Methanol Dehydration to Dimethyl Ether. *Ind. Eng. Chem. Res.* **2019**, *58*, 4042–4053.

[77] Rosas J.M, Rodríguez-Mirasol J, Cordero T. NO reduction on carbon-supported chromium catalysts. *Energ. Fuel.* **2010**, *24*, 3321–3328.

[78] Guerrero-Pérez M.O, Rosas J.M, López-Medina R, Bañares M.A, Rodríguez-Mirasol J, Cordero T. Lignocellulosic-derived catalysts for the selective oxidation of propane. *Catal. Commun.* **2011**, *12*, 989–992.

[79] Bedia J, Ruiz-Rosas R, Rodríguez-Mirasol J, Cordero T. A kinetic study of 2-propanol dehydration on carbon acid catalysts. *J. Catal.* **2010**, *271*, 33–42.

[80] Bedia J, Barrionuevo R, Rodríguez-Mirasol J, Cordero T. Ethanol dehydration to ethylene on acid carbon catalysts. *Appl. Catal. B Environ.* **2011**, *103*, 302–310.

[81] Bedia J, Ruiz-Rosas R, Rodríguez-Mirasol J, Cordero T. Kinetic Study of the Decomposition of 2-Butanol on Carbon-Based Acid Catalyst. *AICHE J.* **2010**, *56*, 1557–1568.

[82] Rashidi S, Esfahani J. A, Hormozi F. Classification of porous materials for energy applications. Reference module in Material Science and Material Engineering, 2020. Doi:10.1016/B978-0-12-803581-8.11739-4

[83] Miller J. R, Burke A. F. Electrochemical Capacitors: Challenges and Opportunities for Real-World Applications. Electrochemical Society Interface, 2008, 17 (1), 53-57. https://www.electrochem.org/dl/interface/spr/spr08/spr08_p53-57.pdf

[84] Ruiz V, Blanco C, Santamaría R, Ramos-Fernández J. M, Martínez-Escandell M, Sepúlveda-Escribano A, Rodríguez-Reinoso F. An activated carbon monolith as an electrode material for supercapacitors. Carbon, 2009,47, 195–200.

[85] Nor NSM, Deraman M, Omar R, Taer E, Awitdrus A , Farma R , Basri NH , Dolah BNM . Nanoporous separators for supercapacitor using activated carbon monolith electrode from oil palm empty fruit bunches. AIP Conf Proc. 2014, 68, 1586. https://doi.org/10.1063/1.4866732

[86] Hasegawa G , Kanamori K , Kiyomura T , Kurata H , Abe T, Nakanishi K. Hierarchically porous carbon monoliths comprising ordered mesoporous nanorod assemblies for high-voltage aqueous supercapacitors. Chem. Mater. 2016, 28, 3944–50.

[87] Moreno-Fernandez G, Kunowsky V, Lillo-Ródenas M. A, Ibañez J, Rojo J. M. New Carbon Monoliths for Supercapacitor Electrodes. Looking at the Double Layer. ChemElectrochem. 2017, 4 (5) 1016. Doi.org/10.1002/celc.201600848.

CHAPTER 2

EXPERIMENTAL

2. EXPERIMENTAL

2.1. ACM preparation

The ACMs were prepared from different biomassic precursors: Alcell® lignin (AL) (Repap Technologies Inc.); eucalyptus Kraft lignin (KL); and olive stone (OS) supplied by S.C.A. Olivarera and Frutera San Isidro, Periana (Málaga). The raw materials were milled and sieved to particle size range of 50-80 μm.

These precursors were impregnated with H_3PO_4 in an impregnation ratio of 1 (H_3PO_4/raw material), and kept in a vacuum dryer for 24 hours, at 60 ºC. In order to study the effect of the impregnation ratio, olive stone was also impregnated with an impregnation ratio of 2. The dried impregnated samples were mixed with distilled water to obtain the adequate rheological properties and plasticity to permit their extrusion. Therefore, the impregnated samples, without any kind of binder, were extruded in an extruder designed by our research group, using a cylindrical mould with an internal diameter of 2 cm, at room temperature and 0.8 MPa. The extruder is composed of different high quality designed die elements (internal diameter of 1 cm), with the aim of obtaining different type of monoliths (compact disc; 25 and 120 channels/cm^2; respectively). When both lignin were used as raw

materials, a stabilization step of the impregnated samples, previous to the extrusion, was necessary to partially avoid the swelling problems. The optimized methods consist of a thermal treatment at 250 ºC, under air flow (150 cm^3/min), for 1 h. Then, 50% of the stabilized material was milled and mixed with 50 % of non-stabilized impregnated lignin, obtaining a paste that finally is extruded to form the monoliths.

Subsequently, the obtained monoliths were activated in a tubular furnace at 700 ºC for 2 h, with a heating rate of 10 ºC/min, under nitrogen flow. Finally, activated monoliths were washed with distilled water at 60 ºC, until constant pH in the eluate.

2.2. Characterization

Ultimate analysis of the samples was performed using a LECO CHNS 932 system, and the corresponding oxygen content was calculated by difference. The ash content of the ACMs was calculated from the weight of the solid residue after being gasified in air at 900 ºC.

The porous texture of the ACMs was evaluated by N_2 adsorption–desorption at -196 ºC and CO_2 adsorption at 0 ºC, using a micrometrics instrument (ASAP 2020 model) and by Hg porosimetry (Autopore IV model). The ACMs were previously outgassed for 8 h at 150 ºC. The

corresponding textural parameters were calculated by applying the BET equation and the t-method from the N_2 isotherm data; and the Dubinin–Radushkevich equation from the CO_2 adsorption data. Narrow pore size distribution of the ACMs was obtained from the N_2 adsorption isotherms by using 2D-NLDFT heterogeneous adsorption models for carbon slit-shaped pores [35]. Macropore size distribution was calculated from Hg porosimetry data.

Surface chemistry of the ACMs was analyzed by temperature-programmed desorption (TPD) and X-ray photoelectron spectroscopy (XPS). CO and CO_2 profiles were obtained in a custom quartz fixed bed reactor placed inside an electrical furnace and quantified by non-dispersive infrared (NDIR) gas analyzers (Siemens ULTRAMAT 22). The samples were heated from room temperature to 930 ºC at a heating rate of 10 ºC/min in N_2 flow. XPS analyses of the samples were obtained by a 5700C model Physical Electronics apparatus, with Mg Kα radiation (1253.6 eV). For the analysis of the XPS peaks, the maximum of the C1s peak was set at 284.5 eV and used as reference for the other peaks.

Acid-base characterization was carried out by analyzing dehydration-dehydrogenation of 2-propanol (IPA-Isopropyl Alcohol) as a model reaction test. The decomposition of IPA was performed under inert

atmosphere and at atmospheric pressure in a quartz fixed bed microreactor (6 mm i.d.) that was placed inside a vertical furnace with temperature control. IPA was fed to the reactor by a syringe pump (Cole-Parmer® 74900-00-05 model, Vernon Hills, IL, USA), ensuring a constant controlled IPA flow, using a partial pressure of IPA of 0.03 atm and a space time of W/F0IPA = 0.1 g·s/µmol. The concentrations of reactant and products were analyzed by gas chromatography (490 micro-GC equipped with PPQ, 5A molsieve, and Wax columns, Agilent Technologies, Santa Clara, CA, USA).

Non-isothermal thermogravimetric analyses were carried out under air atmosphere in a gravimetric thermobalance system, CI electronics. The sample temperature was increased from room temperature up to 900 ºC at a heating rate of 10 ºC/min.

The real density of the ACMs was measured by helium pycnometer using an AccuPyc II 1340 equipment. The evaluation of the mechanical properties of the ACMs (maximum compression strength) was carried out by compression test by using a Deben Microtest tensile stage. The compression rate was 0.003 mm/s. The surface texture and structure of the ACMs were characterized by scanning electron microscopy (SEM),

with a JEOL JSM-6490LV instrument, obtained at a high voltage of 20–25 kV.

The electrochemical performance was studied by using an electrochemical analyzer, model SP- 200 (Bio-Logic Int.) and a standard three electrode cell comprising of a platinum wire as counter electrode, Ag/AgCl electrode as reference electrode and a working electrode that contains the corresponding ACM, which was cut (thickness= 200 μm) and dried at 100ºC in a vacuum oven. Counter collector consists of a stainless steel mesh. Working and counter electrodes were placed face-to-face and tested in 1 M H_2SO_4 electrolyte. Samples were characterized by cyclic voltammetry technique at a scan rate of 1 mV s^{-1} and by galvanostatic charge discharge (GCD) technique from 0 to 0.8 V vs Ag/AgCl/Cl^- 3M until current densities of 1000 mA/g. The capacitances from GCD experiments (Cg^{GCD} and Cv^{GGD}) were calculated from the GCD discharge profile.

The decomposition of methanol was performed in the same microreactor used for IPA decomposition test. The reaction was carried out with 200 mg of ACM, under air atmosphere, at temperatures between 150 and 375 °C. All lines were heated up to 120 °C in order to avoid any condensation. The inlet methanol partial pressure was 0.03 atm and the

water partial pressures were varied from 0 to 0.08 atm, at a space time of 0.1 g·s/µmol.

The outlet gas concentrations were quantified by gas chromatography (490 micro-GC equipped with PPQ, 5A molsieve, and Wax columns, Agilent Technologies, Santa Clara, CA, USA).

The conversion was defined as the ratio of the amount of methanol that was converted to the amount of methanol added to the reactor. The selectivity (in mol%) was defined as the molar ratio of a specific product to the amount of methanol converted. The carbon balance was reached with an error lower than 3% in all cases.

CHAPTER 3

ACTIVATED CARBON MONOLITHS FROM LIGNOCELLULOSIC BIOMASS WASTE FOR ELECTROCHEMICAL APPLICATIONS

3. ACTIVATED CARBON MONOLITHS FROM LIGNOCELLULOSIC BIOMASS WASTE FOR ELECTROCHEMICAL APPLICATIONS

The valorization of lignocellulosic biomass waste into bio-based materials is proposed in this work in order to obtain low-cost materials and to reduce environmental impacts. Cylindrical activated carbon monoliths (ACMs) were prepared from Alcell®, Kraft lignin and olive stone by chemical activation with H_3PO_4. To our best knowledge, there is no previous information about the preparation of ACMs from any type of lignin. In this sense, the development of value-added lignin-based products could be crucial to the economic success of the bio-ethanol production within a biorefinery context.

Therefore, the objective of this chapter is the preparation of binderless ACMs from lignin and olive stones. The first one derived from the pulp and paper industry and new biorefineries for bioethanol production (from lignocellulosic biomass); and the second one obtained from the olive industry. Kraft and Alcell® lignin, and olive stones, impregnated with H_3PO_4, are extruded, and subsequently activated. The obtaining of disks and monoliths with different amount of channels are also evaluated. In order to minimize the possible fusion and swelling of lignin during

activation, different approaches have been tested. Furthermore, the electrochemical properties of the ACMs are analyzed.

3.1. ACMs preparation

The extrusion of the adequate mixing, without any kind of binder, was carried out in a home-made extruder with different dies. Figure 3.1 shows a representation of this extruder designed by our research group for the preparation of the ACMs. The extruder consists mainly of a cylindrical mould of stainless steel with an internal diameter of 2 cm, and different die elements (internal diameter of 1 cm), operated at room temperature. The set-up is able to provide a maximum of 1.6 MPa, although in the preparation of these ACMs, the pressure has not exceeded, in any case 0.8 MPa. Two different die elements were also designed with 19 and 72 pins to obtain monoliths with 25 and 120 channels/cm^2, respectively.

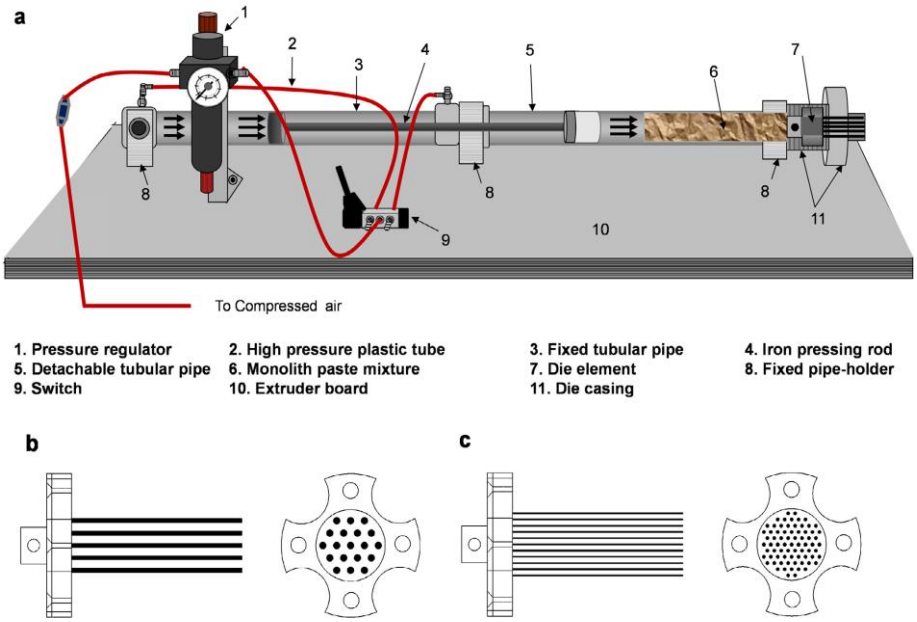

Figure 3.1. a) Components of the home-made extruder designed for the ACM preparation; b) die element with 19 pins and c) with 72 pins, respectively.

3.2. ACMs characterization

Table 3.1 summarizes the ash content and ultimate analysis of the different raw materials. KL presents a high ash content, about 12.4 %, in contrast to AL and OS with very low proportions. AL shows the highest percentage of carbon content (about 65 %). Furthermore, no trace of sulphur is observed in samples AL and OS. In the case of KL, the

significant S (%) is derived from its preparation procedure (Kraft pulping or sulfate process).

Table 3.1. Ash content and ultimate analysis of the different precursors in dry ash free (daf).

Precursor	Ash (%)	C (%)	H (%)	N (%)	S (%)	O (%)*
OS	0.4	48.04	7.32	0.30	n.d.	44.33
AL	0.1	64.80	6.30	0.20	n.d.	28.70
KL	12.4	58.22	6.28	0.11	1.83	33.56

*by difference

The circular shaped monoliths obtained before the activation step present a cross section with a diameter of 0.9 cm. **Figure 3.2** shows some SEM micrographs of the different types of AL monoliths. As can be seen, the configuration of the extruder allows for obtaining disks and monoliths with 25 and 120 channels/cm^2 at very low pressure (0.8 MPa) compared to those reported in the literature obtained at 130 MPa [1,2]. ACMs undergo shrinkage of their sizes after the activation step. For instance, the diameter of the cross sectional view in the monoliths OS and AL at the same impregnation ratio, are reduced to approximately 25%. In general, the density cell of the different ACMs varies from 30 to 125 cell/cm^2, the wall thickness was from 250 to 800 μm, the hydraulic

diameter was from 0.7 to 4 cm, the open frontal area was between 5 and 25 %, and the geometric surface area varies from 0.7 to 1 cm^2/cm^3.

Figure 3.3 represents some SEM micrographs of the ACMs disks for the different raw materials: OS, AL, KL. It is important to mention that the ACMs obtained from lignin needed a previous stabilization treatment to avoid swelling during the activation step. As can be seen, OS and AL monoliths appeared to be very similar. In contrast, Kraft lignin monolith shows more similar xerogel-like morphology as shown in Fig. 3.3(c).

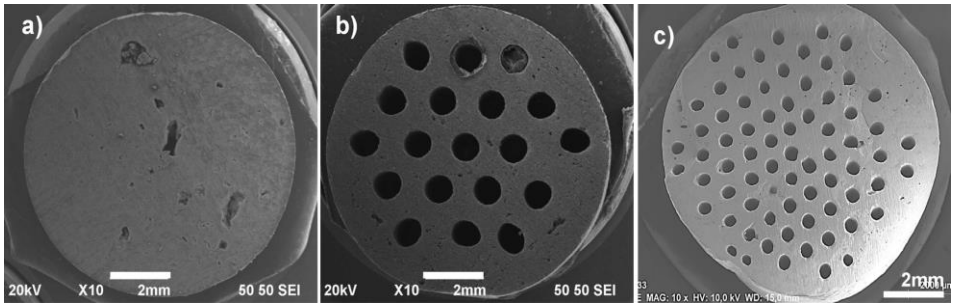

Figure 3.2. SEM micrographs of the Alcell lignin monoliths a) carbon disk; b) monolith with 25 channels/cm^2; c) monolith with 120 channels/cm^2.

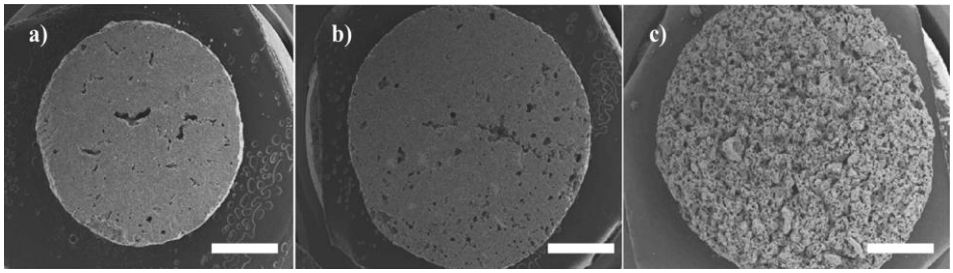

Figure 3.3. SEM micrographs of the activated carbon monoliths disks from OS1; AL1; and KL1, respectively. Bar length: 2 mm.

Table 3.2 shows the yields and ultimate analyses of the ACMs. Yield is related to the composition of the raw material, i.e. hemicellulose, cellulose and lignin content. The highly aromatic and carbon-rich molecular structure of lignin devolatilizes to a lesser extent than cellulose and hemicelluloses [3]. In this sense, olive stones contain approximately 26–32% of lignin [4], which explains the lower yield of this monolith compared to that of Alcell lignin. In the case of Kraft lignin, the high ash content of this precursor is a probable explanation of its yield, which can be also directly related to the lowest carbon content obtained by the ultimate analysis. On the other hand, yields of OS, AL and KL monoliths are similar to those reported for different AC by Yakout et al., from OS [5]; Rosas et al., from AL [6], and Montane et al., from KL [7] respectively. Although these last ACs were obtained at different impregnation ratios. As expected, the yield of OS monoliths decreases

with the impregnation ratio, as a consequence of a deeper dehydration of the carbonaceous structure of the precursor [8], and the corresponding carbon content increases [9-10]. These results suggest that the conformation into monoliths does not produce any significant influence of the yields of the obtained ACMs.

Table 3.2. Yields and ultimate analyses of the ACMs in dry ash free (daf).

Monoliths	Yield (%)	C (%)	H (%)	N (%)	S (%)	O (%)*
OS1	39.5	78.96	3.73	0.31	n.d.	16.99
OS2	28.8	81.72	3.26	0.42	n.d.	14.60
AL1	40.5	86.26	3.95	0.31	n.d.	9.47
KL1	32.0	78.22	3.47	0.22	0.98	17.12

*by difference, includes P content.

Figure 3.4 represents the N_2 adsorption-desorption isotherms of the ACMs disks at -196 ºC. It is important to mention that no significant differences were found in the N_2 adsorption-desorption isotherms of the different type of monoliths (disks; 25 and 120 channels/cm^2) from the same precursor. ACMs obtained from both Kraft and Alcell lignin show type I isotherms characteristic of typical microporous solids, where almost all N_2 volume adsorbed takes place at low relative pressures.

Specifically, Kraft lignin-derived monolith presents a more pronounced horizontal plateau, starting at very low relative pressure, indicating the presence of narrower microporosity. The monoliths obtained from olive stone show a type IV isotherm with an increase of the adsorbed volume in the entire relative pressure range, in general, the sample obtained at higher impregnation ratio presents a large amount of porosity with microporous and mesoporous structures. As it is well known, the increase of the relative amount of activation agent generates a higher development of porosity, widening the porous structure of the monoliths [1].

On the other hand, the porosity development of the ACMs, at the same impregnation ratio, follows the sequence: OS>AL>KL, probably due to the presence of cellulose in OS. In this line, Guo and Rockstraw pointed out the great influence of the precursor in the porosity development, showing higher surface areas in carbons obtained from cellulose than those from Kraft lignin, at impregnation ratios equal or higher than 1 [11].

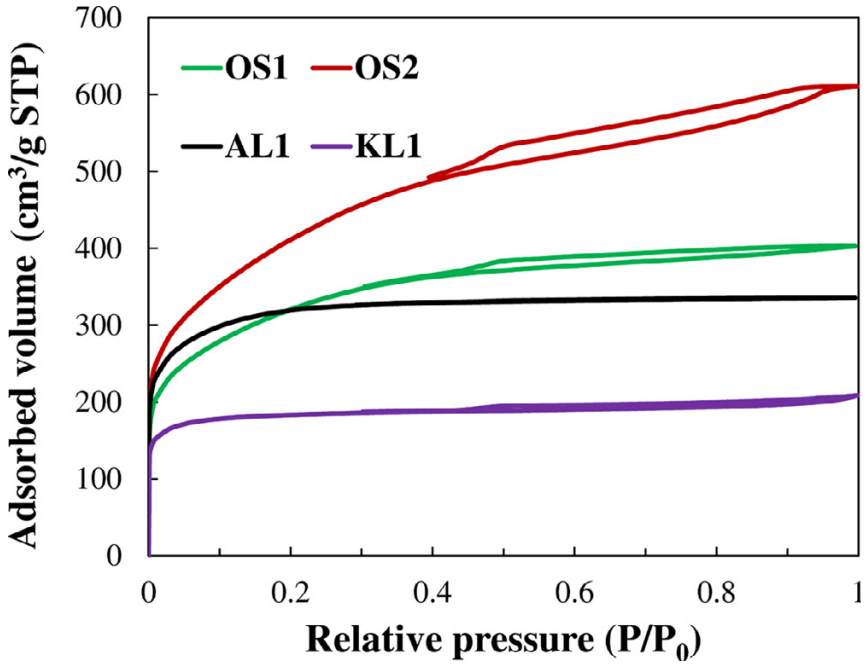

Figure 3.4. N_2 adsorption-desorption isotherms of the ACMs disks at -196 ºC.

With regard to the macroporosity, shown in the right side of the figure, the features observed in SEM micrographs are corroborated in the PSD, and the monolith from Kraft lignin exhibits the highest contribution of macroporosity. In contrast, the presence of macropores in monoliths from olive stone is lower than that in monoliths from lignin. The left side of the figure shows the PSD obtained from N_2 adsorption-desorption at -196 ºC. A broad pore size distribution was observed in all cases. All the ACMs present a predominant peak center around 0.7 nm and a second

peak at pore sizes between 1.4 and 2.0 nm. The monoliths prepared from Kraft and Alcell lignin show a bimodal distribution in the micropore range. In the case of ACMs prepared from olive stone (OS1 and OS2), a wider pore size distribution is observed, obtaining mesopores up to 4 nm. This effect is more noticeable in the sample OS2 due to the higher impregnation ratio, which produces a broadening of the porosity.

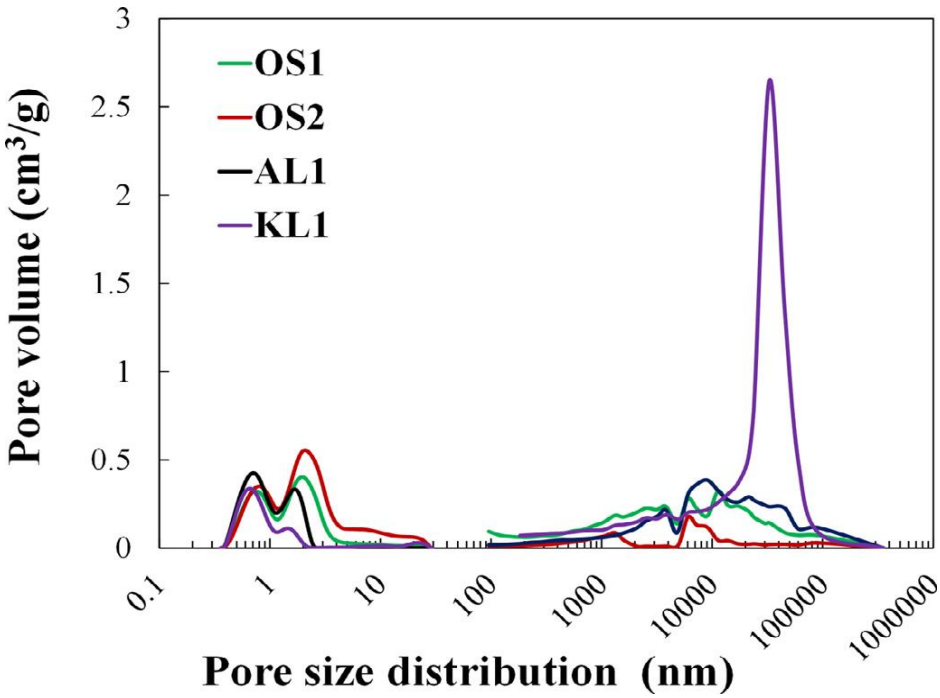

Figure 3.5. Pore size distribution (PSD) of the ACMs disks derived from both the N_2 adsorption-desorption at -196 ºC and Hg porosimetry.

Table 3.3 summarizes the textural parameters of the ACMs. The porosity percentage, true density and the maximum compression strength were also collected in this table. The monoliths exhibit apparent surface areas (A_{BET}) between 700 and 1500 m^2/g, which indicate the well-developed porous structure produced after the activation step. ACMs prepared from lignin (AL1 and KL1) present lower values of external area (A_t) and mesopore volume (V_{mes}). On the other hand, when olive stone is used as precursor, higher external surface area and mesopore volume are observed, obtaining at the impregnation ratio of 2, A_t=300 m^2/g and V_{mes}=0.35 cm^3/g. Micropore volumes derived from CO_2 adsorption at 0 ºC are quite similar in all monoliths, ranging around 0.25 cm^3/g. For the sake of comparison, activated carbons obtained at the same experimental conditions than those used for monoliths were also prepared. The analysis of the porosity suggests that the extrusion does not modify substantially the porous structure of the activated carbon, even in some cases, a slight increase of the apparent surface area was observed.

As aforementioned, there is certain lack of knowledge about the preparation of ACM from lignin. However, there are some works related to the obtaining of ACM from olive stones. In this sense, the values of the apparent surfaces area are higher than some pellets reported in the

literature [12], and the micropore volumes are in the same order than others [13]. In any case, the possibility of obtaining monoliths not only with higher porosity development, but also with different amount of channels, is an additional advantage compared to pellets, since the pressure drop associated to some applications, such as like adsorbents or catalysts, could make these ACMs into quite attractive materials. Specifically in electrochemical applications, the contact between particles in monoliths is much better than that observed in pellets made from compaction under pressure of a powdered carbon [14].

The density of monoliths is also of great interest, overall, in the gas storage applications, where adsorption on a volumetric basis is an important design parameter [15]. The true density of the monoliths is around 1.75 g/cm^3, but an increase of this value can be observed from OS to KL, at the same impregnation ratio. The true density of OS also increases with the impregnation ratio, as a consequence of the dehydration reaction at low temperature that would facilitate further repolimerization and condensation reaction and conversion to carbon [13]. The values obtained from the different precursors are quite similar to those reported in the literature from different lignocellulosic precursors [2, 13]. It is important to point out that the monolith (from Kraft lignin) with higher true density also shows the highest porosity

percentage, 64%. A relevant parameter in electrochemical applications is the bulk density, which can be calculated from the porosity and the true density. The values here obtained are ranging from 0.7 for KL1 to 1.4 g /cm^3 for OS1, these values are considerably higher than others reported in the literature with monoliths obtained by compression of a powdered carbon [16-17]. With regard to the mechanical strength of ACMs, the compression strength values observed are in the same range than those reported for different raw materials, with the highest value found for that obtained from Alcell lignin with 7.56 MPa [14,18,19].

Table 3.3. Textural parameters, true densities and maximum compression strength values of the ACMs.

Sample	N_2 adsorption				CO_2 adsorption		Ø (%)	ρ_{Tavg}^{He} (g/cm^3)	Maximum compression strength (MPa)
	A_{BET} (m^2/g)	V_t (cm^3/g)	A_t (m^2/g)	V_{mes} (cm^3/g)	A_{DR} (m^2/g)	V_{DR} (cm^3/g)			
OS1	1147	0.50	115	0.12	622	0.25	17.5	1.69	5.88
OS2	1489	0.59	297	0.35	638	0.26	48.0	1.82	7.36
AL1	1054	0.49	29	0.02	734	0.29	38.9	1.77	7.56
KL1	682	0.28	23	0.09	569	0.23	63.8	1.85	4.12

Figure 3.6 shows the CO (a) and CO_2 (b) evolution from TPD analyses of the different ACMs. The activated carbon monoliths show most of the CO evolution at high temperatures, which can be attributed to the presence of C-O-PO_3 groups formed during the activation of phosphoric acid, as reported by our research group in previous studies [6, 20]. Wu and Radovic also reported the formation of this kind of groups by impregnating carbon/carbon composite samples with a methanol solution of methyl-phosphonic acid or phosphorus oxychloride and heating at ca. 600 ºC [21]. A lower amount of CO is desorbed at temperatures below 700 ºC, due to decomposition of anhydride, phenol and ether groups. The amount of CO_2 evolved (Fig. 3.6.b) from the ACMs is significantly lower than that corresponding to CO evolution, indicating a lower concentration of carboxyl, lactonic and anhydride surface groups. The monolith with the highest presence of CO- evolving groups is that from Kraft lignin. This feature is quite relevant, because the surface oxygen groups that decompose as CO are reported to be more electrochemically active than CO_2- evolving groups, which can actively contribute to charge storage by pseudocapacitive reactions [22]. The total amounts of CO and CO_2 released during the TPD analyses are also summarized in Table 3.4. As can be seen, the amounts of CO desorbed are significantly higher for the sample KL1, and very similar for the AL1

and OS2 carbon monoliths. This table also collects the weight surface composition of the ACMs determined from XPS analyses. The ACMs show carbon surface concentrations higher than 78%, oxygen concentrations from 7.8 to 18.8% and phosphorus concentrations higher than 2%, with the highest value found for the KL1 monolith.

Figure 3.7 shows P2p spectra of the different ACMs. Three main species of phosphorus can be detected at 134.1 eV related to the presence of –C–O–PO_3, –$(CO)_2$–PO_2 or –$(CO)_3$–PO species; at 133.1 eV associated to –C–PO_3 or –C_2–PO_2 species and; at 132 eV attributed to reduced –C_3–PO species [23]. As can be seen, KL1 monolith presents the highest contribution of the more oxidized phosphorus species; meanwhile AL1 monolith shows the highest proportion of the more reduced ones.

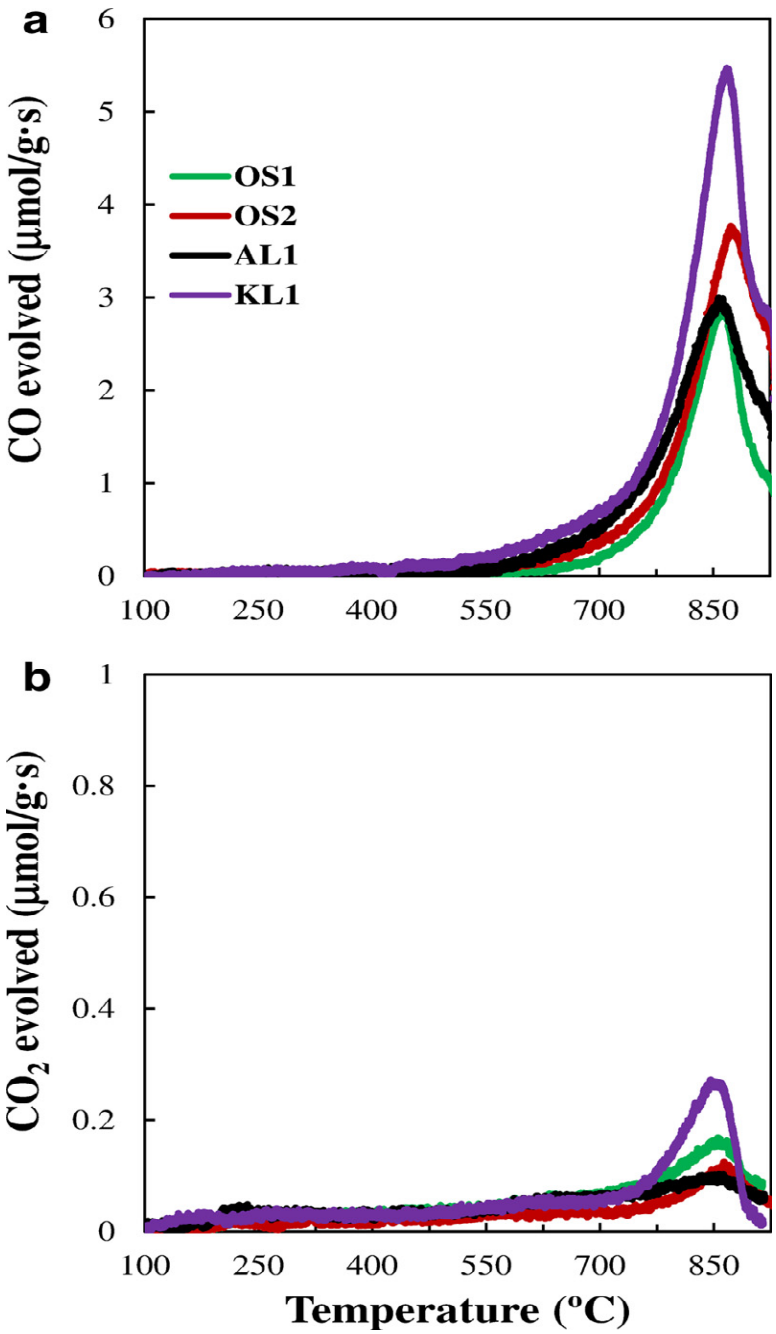

Figure 3.6. CO (a) and CO_2 (b) evolution during the TPD of the different ACMs disks.

Table 3.4. Weight surface concentration determined by XPS and CO and CO_2 evolved from TPD analyses

ACM	XPS				TPD	
	C (%wt)	O (%wt)	P (%wt)	S (%wt)	CO (mmol/g)	CO_2 (mmmol/g)
OS1	87.2	11.6	2.8	0.0	5.5	0.6
OS2	89.0	7.8	3.2	0.0	6.4	0.4
AL1	87.3	9.0	3.7	0.0	6.1	0.5
KL1	78.4	16.7	4.5	0.3	9.5	0.7

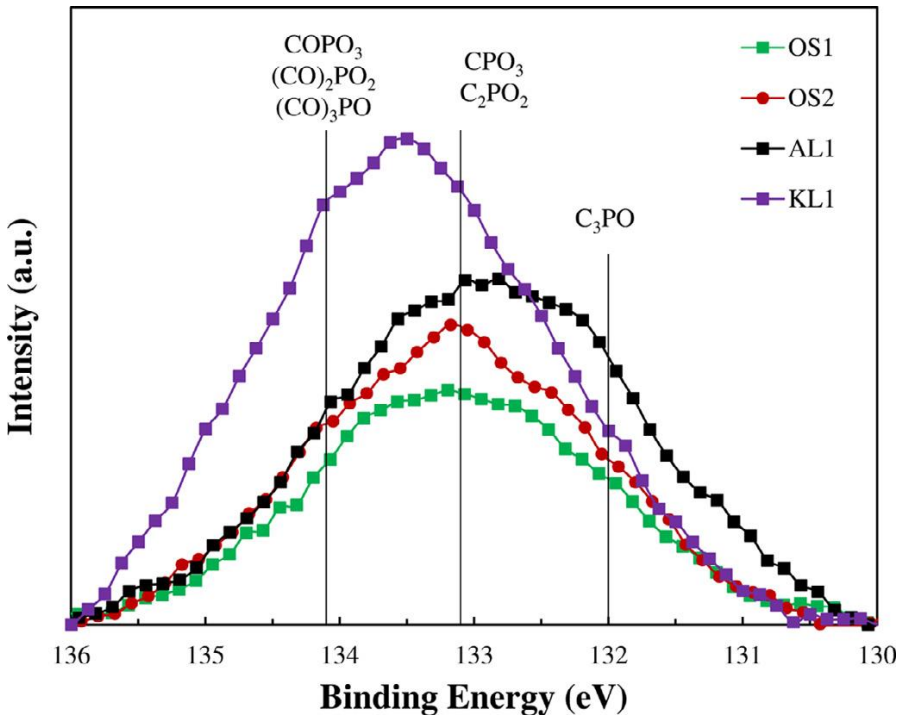

Figure 3.7. P2p spectra for the different ACMs.

In order to further analyze the behavior of these ACMs under oxidizing conditions, non-isothermal oxidation experiments were carried out. Figure 3.8 shows the non-isothermal oxidation resistance profiles or the different ACMs. In general, all the ACMs started to oxidize significantly at temperatures below 500 ºC. As it was previously reported, the presence of thermally stable phosphorus complexes that remain on the carbon surface after the activation process is the responsible of the high oxidation resistance of these ACMs [6, 20]. In this sense, the weight gain noticed between 350 and 500 ºC can be related to the oxidation of the more reduced phosphorus species (–C_3–PO groups) into C–O–PO_3 species, which is subsequently followed by a significant weight loss associated to the carbon gasification [6]. The KL1 monolith presents a slightly lower oxidation resistance compared to the other ACMs. The majority presence of oxidized species in the parent KL1 can be a possible explanation of this tendency.

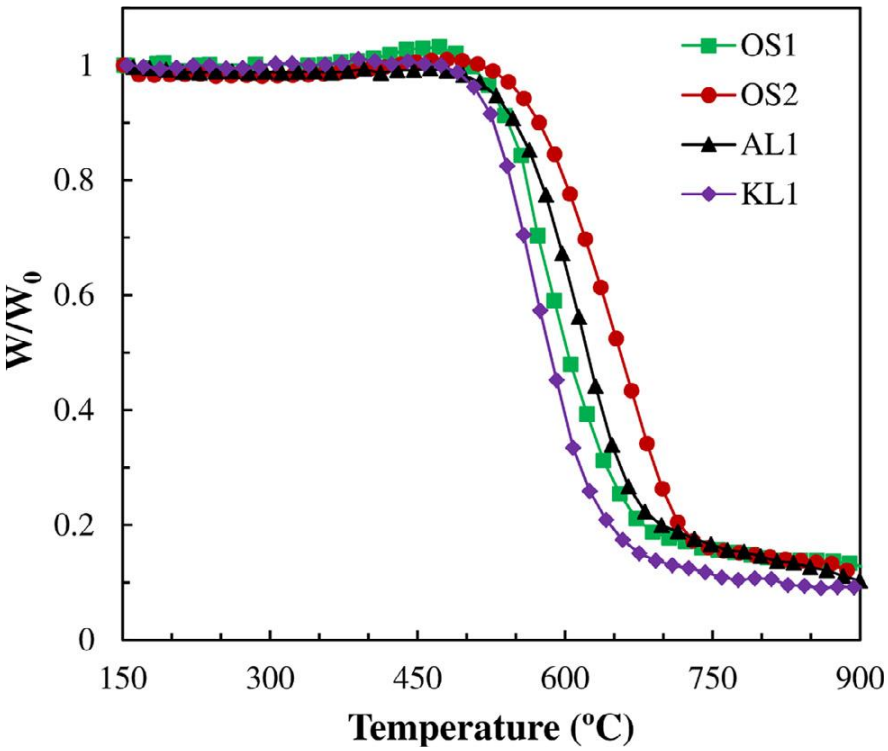

Figure 3.8. Non-isothermal oxidation resistances profiles for the different ACMs.

3.3. Electrochemical characterization

ACMs disks were tested in a three electrode cell with H_2SO_4 as electrolyte to evaluate their electrochemical performance. Cyclic voltammetries were carried out for the potential window from 0 to 0.8 V, at a scan rate of 1 mV/s. Figure 3.9.a shows the cyclic voltammograms of ACMs and 3.9.b the corresponding galvanostatic charge-discharge curves. ACM electrode from OS2 exhibits the highest current responses

at this scan rate, followed by the KL1, AL1 and OS1 monolith. Based on the mechanism of double-layer charge/discharge, the specific capacitance of the ACMs should be directly proportional to their apparent surface area (A_{BET}) [24]. In that case, OS2 also presents the highest surface area and pore volume. However, KL1 shows a remarkable electrochemical performance in spite of its low surface area and pore volume. This anomalous result suggests that the specific capacitance of the ACMs was not only contributed by the double-layer charge/discharge at the electrode–electrolyte interface but also by the redox transitions of surface functional groups (i.e., pseudo-capacitance) [25] and/or by the differences of the starting material [26]. In this sense, the reversible redox peak at 0.38 V can be associated to the reversible quinone/hidroquinone groups on the carbon surface. This peak can correspond to the presence of quinone C=O and P=O polyphosphates [27-28]. In fact, KL1 presents the highest amount of surface functional groups, which desorb as CO during TPD (as reported in Table 3.4), and the highest P content determined by XPS analyses (see also Table 3.4).

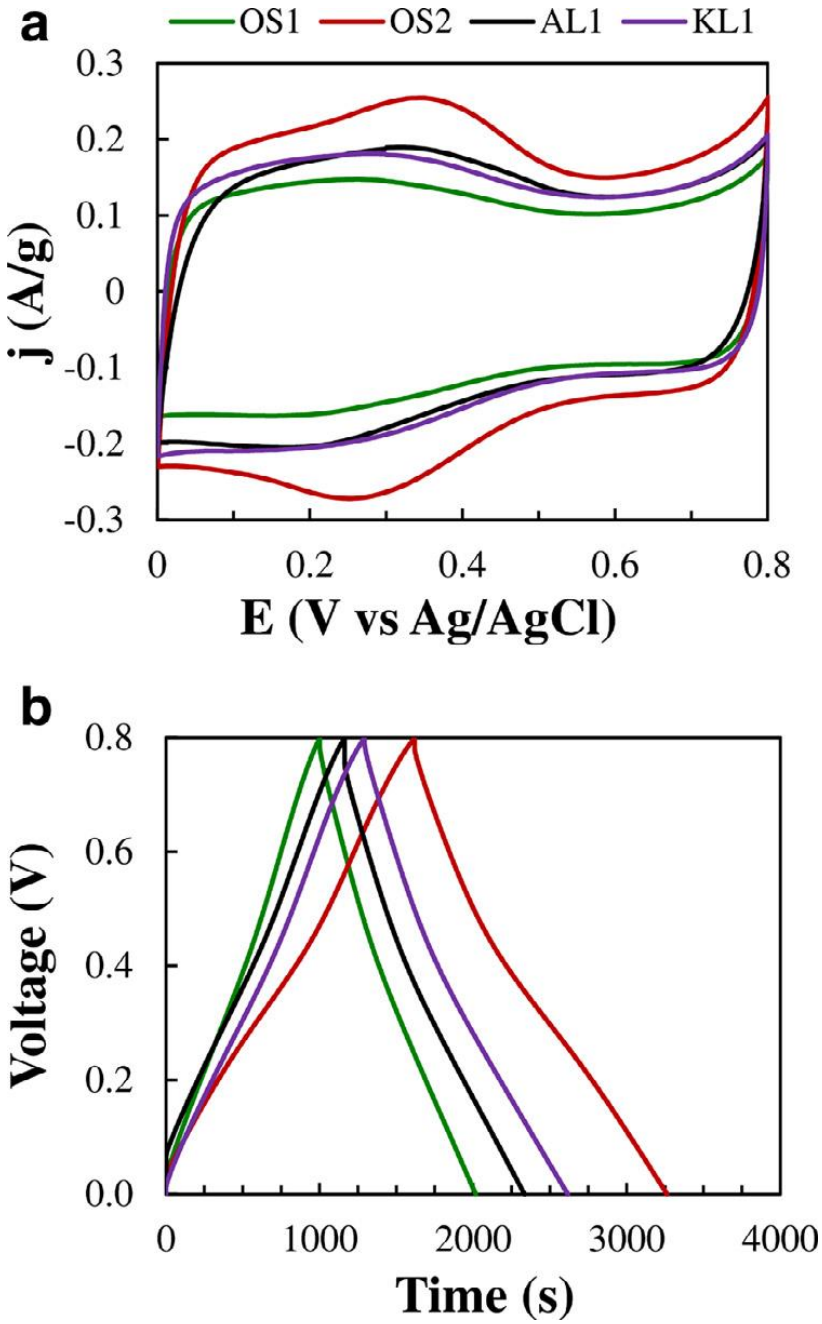

Figure 3.9.(a) Voltammogram data obtained at 1 mV·s^{-1}; (b) Galvanostatic charge-discharge curves at 50 mA/g for the different ACMs disks.

The constant current charge-discharge studies of the supercapacitor cell were performed between cell voltages of 0 and 0.8 V, at different discharge current densities between 50 and 1000 mA/g (see Figure 3.9.b). Although P- carbons have shown high electrogasification resistance, being able to operate at potentials larger than 1.2 V [29-31], the relatively mild conditions used in this work were selected to ensure the stability of the electrodes, avoiding their partial electrogasification [32]. The shape of the charge–discharge curves are closely linear and show a typical symmetric triangular distribution, indicating a good double layer capacitive property. Comparative values of specific capacitance from galvanostatic charge-discharge and cyclic voltammetry are listed in Table 3.5 for all the ACMs electrodes. The different methods to calculate specific capacitances reveal the same tendency. There is not a clear relationship between the specific capacitance values and the apparent surface area, suggesting the great influence of the type of precursor and the pseudo-capacitance.

Table 3.5. Specific and volumetric capacitances obtained from cyclic voltammetry (CV), at 1mV/s, and constant current charge-discharge (GCD), at 50 mA/g, of the ACMs electrodes.

Electrodes	C_g^{CV} (F/g)	C_g^{GCD} (F/g)	C_v^{GCD} (F/cm^3)
OS1	122	134	187
OS2	191	217	205
AL1	144	161	174
KL1	151	166	111

Table 3.6 shows a comparison of the specific and volumetric capacitances of different ACMs. The values of specific capacitances for the ACMs are comparable or even better than others reported in the literature with similar porosity, but the volumetric capacitances of OS2 and AL1 are considerably higher than the values obtained at similar conditions by other authors. Furthermore, the advantage of these materials is the use of a simple preparation method to obtain ACM electrodes from biomass waste precursors.

Table 3.6. Specific and volumetric capacitances of different ACMs reported in the literature.

Raw material	Specific capacitance (F/g)	Volumetric capacitance (F/cm^3)	Reference
Anthracite/polymer	300	167	[11]
Eucalyptus grandis wood	187	80	[16]
Ethylene-tar	334	<167	[33]
Oil palm empty fruit bunches	122	n.p.*	[34]
Fir wood	197	n.p.*	[24]
Rubber wood sawdust	138	80	[35]
Self-adhesive carbon grains	150	n.p.*	[36]
Oil palm empty fruit bunches	< 100	n.p.*	[37]
Rubber wood waste	129	104	[38]
Phenolic resins	206	111	[39]
Olive stone	217	205	This work
Alcell lignin	161	174	This work

*not provided

Figure 3.10 collects the evolution of the C_g of the different ACMs as a function of the current density. A reduction of Cg values of approximately 30% is observed at current densities as high as 1 A/g for almost all ACMs, excepting for KL1, which shows a decrease of the specific capacitance around 40%. This trend can be associated to a higher

contact resistance between the current collector and the KL1 electrode, associated to its xerogel-like morphology and its high porosity value (see Table 3.3). In addition, the most stable electrode is OS2, which maintains a capacitance value of 150 F/g at this relatively high current density (1 A/g). As can be seen, this value can be still considered significant, when it is compared to the specific capacitances shown in Table 3.6.

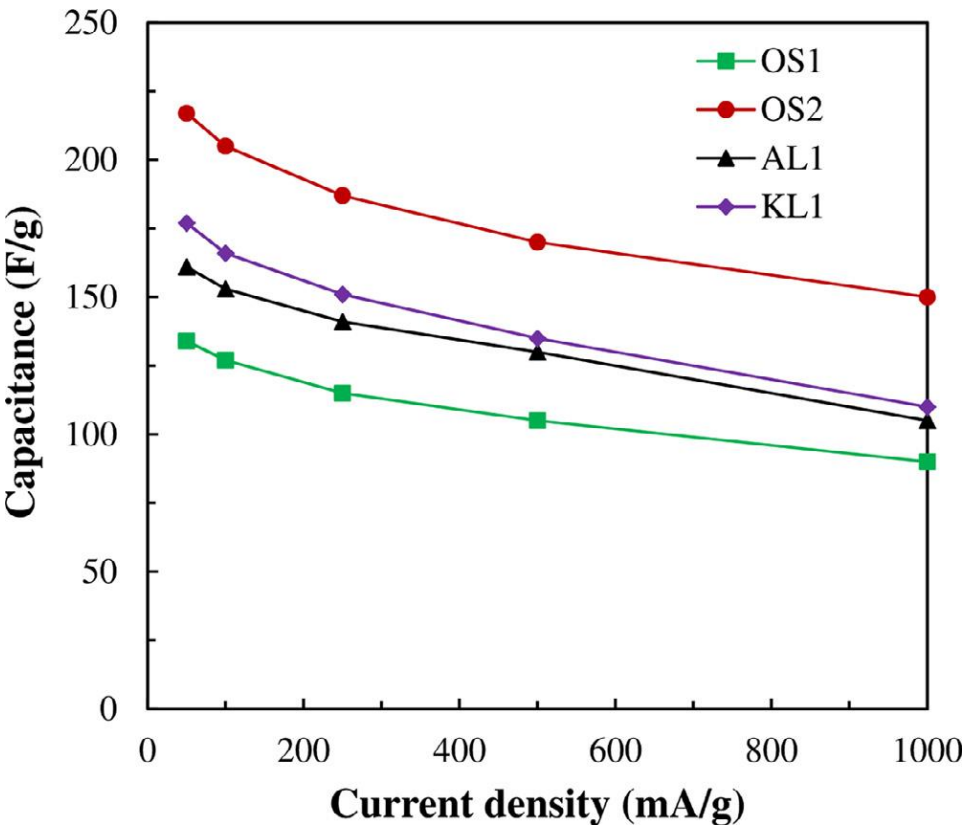

Figure 3.10. Evolution of the specific capacitance as a function of the current density for all the ACMs.

3.4 Conclusions

A series of cylindrical activated carbon monoliths (ACMs) were prepared by chemical activation of different lignocellulosic biomass waste such as olive stone, Alcell and kraft lignin with phosphoric acid at different impregnation ratios. To our best knowledge, there is no previous information about the preparation of ACMs from any type of lignin. The extrusion of the adequate mixing, without any kind of binder, was carried out in a home-made extruder with different die elements. This method allows for obtaining disks and monoliths with 25 and 120 channels/cm^2.

In the case of lignin precursors, a stabilization step becomes necessary to minimize the problems of plasticity and swelling. Half of the impregnated sample is treated at 250 ºC in air and mixed to the rest of impregnated sample before the extrusion. This method is valid for Alcell lignin. In the case of Kraft lignin, a partial contraction of the size is noticed. An activated micropore carbon monolith with an apparent surface area of about 1500 m^2/g, with micropore volume of 0.538 cm^3/g was obtained at 700 ºC with an impregnation ratio of 2, using olive stone as precursor. The bulk density of the monoliths is also very high (~1.1 g/cm^3 for ACM from Alcell lignin), with compression strength of 7.6

MPa. This high density opens the whole range of possibilities for different applications.

Electrochemical characterization was carried out by cyclic voltammetry and galvanostatic charge-discharge techniques with electrodes from ACMs in the absence of any type of binder and conductivity promoter. The olive stone monolith presents the highest specific capacitance of all the ACMs, approximately 217 F/g. (volumetric capacitance of 205 F/cm^3). This value is higher than others reported in the literature for activated carbons obtained from lignocellulosic precursors.

3.5 References

[1] Molina-Sabio M, Rodríguez-Reinoso F, Caturla F, Sellés MJ. Porosity in granular carbons activated with phosphoric acid. Carbon 1995;33:1105–13 .

[2] Nakagawa Y, Molina-Sabio M, Rodríguez-Reinoso F. Modification of the porous structure along the preparation of activated carbon monoliths with H_3PO_4 and $ZnCl_2$. Microporous Mesoporous Mater 2007;103:29–34 .

[3] Rosas JM, Bedia J, Rodriguez-Mirasol J, Cordero T. Preparation of hemp-derived activated carbon monoliths. Adsorption of water vapor. Ind Eng Chem Res 2008;47:1288–96 .

[4] Rodríguez G, Lama A, Rodríguez , Jiménez A, Guillén R, Fernández-Bolaños J. Olive stone an attractive source of bioactive and valuable compounds. Bioresour Technol 2008;99:5261–9 .

[5] Yakout SM, Sharaf El-Deen G. Characterization of activated carbon prepared by phosphoric acid activation of olive stones. Arab J Chem 2016;9:S1155–62 .

[6] Rosas JM, Ruiz-Rosas R, Rodríguez-Mirasol J, Cordero T. Kinetic study of the oxidation resistance of phosphorus-containing activated carbons. Carbon 2012;50:1523–37 .

[7] Montané D, Torné-Fernández V, Fierro V. Activated carbons from lignin: kinetic modeling of the pyrolysis of Kraft lignin activated with phosphoric acid. Chem Eng J 2005;106:1–12 .

[8] Jagtoyen M, Derbyshire F. Activated carbons from yellow poplar and white oak by H3PO4 activation. Carbon 1998;36:1085–97 .

[9] Williams PT, Reed AR. Pre-formed activated carbon matting derived from the pyrolysis of biomass natural fiber textile waste. J Anal Appl Pyrolysis 2003;70:563–77 .

[10] Williams PT, Reed AR. High grade activated carbon matting derived from the chemical activation and pyrolysis of natural fibre textile waste. J Anal Appl Pyrolysis 2004;71:971–86 .

[11] Guo Y, Rockstraw DA. Physical and chemical properties of carbons synthe- sized from xylan, cellulose, and Kraft lignin by H_3PO_4 activation. Carbon 2006;44:1464–75

[12] Djeridi W, Ouederni A, Wiersum AD, Llewellyn PL, El Mir L. High pressure methane adsorption on microporous carbon monoliths prepared by olives stones. Mater Lett 2013;99:184–7.

[13] Molina-Sabio M, Almansa C, Rodríguez-Reinoso F. Phosphoric acid activated carbon disks for methane adsorption. Carbon 2003;41:2113–19 .

[14] Moreno-Fernandez G, Kunowsky M, Lillo-Rodenas MA, Ibañez J, Rojo JM. New carbon monoliths for supercapacitor electrodes. Looking at the double layer. ChemElectroChem 2017;4:1016–25 .

[15] Marco-Lozar JP, Kunowsky M, Suárez-García F, Carruthers JD, Linares-Solano A. Activated carbon monoliths for gas storage at room temperature. Energy Environ Sci 2012;5:9833–42 .

[16] Hasegara G, Kanamori K, Kiyomura T, Kurata H, Abe T, Nakanishi K. Hierarchically porous carbon monoliths comprising ordered mesoporous nanorod assemblies for high-voltage aqueous supercapacitors. Chem Mater 2016;18:3944–50 .

[17] Cuña A, Ortega Vega MR, da Silva EL, Tancredi N, Radtke C, Malfatti CF. Nitric acid functionalization of carbon monoliths for

supercapacitors: effect on the electrochemical properties. Int J Hydrog Energy 2016;41:12127–35 .

[18] Lozano-Castelló D, Cazorla-Amorós D, Linares-Solano A, Quinn DF. Activated carbon monoliths for methane storage: influence of binder. Carbon 2002;40:2817–25 .

[19] Li DC, Ding JW, Qian TT, Zhang S, Jiang H. Preparation of high adsorption performance and stable biochar granules by $FeCl_3$ -catalyzed fast pyrolysis. RSC Adv 2016;6:12226–34 .

[20] Rosas JM, Bedia J, Rodríguez-Mirasol J, Cordero T. Hemp-derived activated carbon fibers by chemical activation with phosphoric acid. Fuel 2009;88: 19–26.

[21] Wu X, Radovic LR. Inhibition of catalytic oxidation of carbon/carbon composites by phosphorus. Carbon 2006;44:141–51 .

[22] Bleda-Martínez MJ, Maciá-Agulló JA, Lozano-Castelló D, Morallón E, Cazorla-Amorós D, Linares-Solano A . Role of surface chemistry on electric double layer capacitance of carbon materials. Carbon 2005;43:2677–84 .

[23] Cordero-Lanzac T, García-Mateos FJ, Rosas JM, Rodriguez-Mirasol J, Cordero T. Flexible binderless capacitors based on P- and N-

containing fibrous activated carbons from denim cloth waste. Carbon 2018;139:599–608 .

[24] Kinoshita K. Carbon, electrochemical and physicochemical properties. John-Wiley & Sons New York; 1988.

[25] Wu FC, Tseng RL, Hu CC, Wang CC. The capacitive characteristics of activated carbons comparisons of the activation methods on the pore structure and effects of the pore structure and electrolyte on the capacitive performance. J Power Sources 2006;159:1532–42 .

[26] Wu FC, Tseng RL, Hu CC, Wang CC. Effects of pore structure and electrolyte on the capacitive characteristics of steam- and KOH-activated carbons for supercapacitors. J Power Sources 2005;144:302–9 .

[27] Huang C, Puziy AM, Sun T, Poddubnaya OI, Suárez-García F, Tascon JMD, Hulicova-Jurcakova D. Capacitive behaviours of phosphorus-rich carbons derived from lignocelluloses. Electrochemical Acta 2014;137:219–27 .

[28] Huang C, Sun T, Hulicova-Jurcakova D. Wide electrochemical window of supercapacitors from coffee bean-derived phosphorus-rich carbons. ChemSusChem 2013;6:2330–9 .

[29] Hulicova-Jurcakova D, Puziy AM , Poddubnaya OI , Suárez-García F , Tascón JMD , Lu GQ. Highly stable performance of supercapacitors from phosphorus-enriched carbons. J Am Chem Soc 2009;131:5026–7

[30] Calvo EG, Lufrano F, Arenillas A, Brigandì A, Menéndez JA, Staiti P. Effect of un-equal load of carbon xerogel in electrodes on the electrochemical performance of asymmetric supercapacitors. J Appl Electrochem 2014;44:481–9 .

[31] Liu C, Li C, Ahmed K, Mutlu Z, Lee I, Zaera F, et al. High-potential metalless nanocarbon foam supercapacitors operating in aqueous electrolyte. Small 2018;14:17024 4 4.

[32] Berenguer R, Ruiz-Rosas R, Gallardo A, Cazorla-Amoros D, Morallon E, Nishihara H, Kyotani T, Rodriguez-Mirasol J, Cordero T. Enhanced electro-oxidation resistance of carbon electrodes induced by phosphorus surface groups. Carbon 2015;95 6 81-6 89 .

[33] Gutierrez MC, Rosas JM, Rodríguez-Cano MA, Luque I, Rodriguez-Mirasol J, Cordero T . Strategic situation, design and simulation of a biorefinery in Andalusia. Energy Convers Manag 2019;182:201–14 .

[34] Ruiz V, Blanco C, Santamaría R, Ramos-Fernández JM, Martínez-Escandell M, Sepúlveda-Escribano A, Rodríguez-Reinoso F. An activated carbon monolith as an electrode material for supercapacitors. Carbon 2009;47:195–200 .

[35] Taer E, Deraman M, Talib IA, Awitdrus A, Hashmi SA, Umar AA. Preparation of a highly porous binderless activated carbon monolith from rubber wood sawdust by a multi-step activation process for application in supercapacitors. Int J Electrochem Sci 2011;6:3301–15.

[36] Farma R, Deraman M, Awitdrus A, Talib IA, Taer E, Basri NH, Manjunatha JG, Ishak MM, Dollah BNM, Hashmi SA. Preparation of highly porous binderless activated carbon electrodes from fibres of oil palm empty fruit bunches for application in supercapacitors. Bioresource Technol 2013;132:254–61 .

[37] Nor NSM, Deraman M, Suleman M, Jasni MRM, Manjunatha JG, Othman MAR Shamsudin SA. Supercapacitors using binderless activated carbon monoliths electrodes consisting of a graphite additive and pre-carbonized biomass fibers. Int J Electrochem Sci 2017;12:2520–39 .

[38] Thubsuang U, Laebang S, Manmuanpom N, Wongkasemjit S, Chaisuwan T. Tuning pore characteristics of porous carbon monoliths prepared from rubber wood waste treated with H_3PO_4 or NaOH and their potential as supercapacitor electrode materials. J Mater Sci 2017;52:6837–55

[39] Moreno-Fernandez G, Ibañez J, Rojo JM, Kunosky M. Activated carbon fiber monoliths as supercapacitor electrodes. Adv Mater Sci Eng 2017;2017, Article ID 3625414.

CHAPTER 4

ACID MESOPOROUS CARBON MONOLITHS FROM LIGNOCELLULOSIC BIOMASS WASTE FOR METHANOL DEHYDRATION

4. ACID MESOPOROUS CARBON MONOLITHS FROM LIGNOCELLULOSIC BIOMASS WASTE FOR METHANOL DEHYDRATION

In this chapter, ACMs with axial channels were prepared from the direct extrusion of different lignocellulosic materials, Alcell, Kraft lignin and olives stones, impregnated with phosphoric acid, followed by activation at 700 °C. The activity and stability of these ACMs were analyzed for methanol dehydration reaction in air atmosphere. The influence of the presence of water on the dehydration of methanol were also studied. A kinetic model was also proposed to reproduce the experimental results.

4.1. ACMs Characterization

Cylindrical ACMs were obtained with preparations yields that ranged from 30 to 40% (ACMs mass/raw material mass). Figure 4.1 shows SEM micrographs of the ACMs obtained from olive stone, Alcell lignin and Kraft lignin, at an impregnation ratio of 1. The ACMs from olive stone and Alcell lignin presented a cross section diameter of approximately 0.7 and 0.8 cm, with cell densities of 54 and 38 channels/cm^2, respectively (see Figures 4.1a,d). Details regarding the channels of both ACMs showed quite regular circular hollows along all the length of the monolith, with channel sizes ranging from 700 to 800 µm. In case of

Kraft lignin derived activated carbon monolith, a more similar xerogel-like morphology was obtained, making the channels practically indiscernible, due to their collapse during the heat treatment at 700 °C. Accordingly, only discs were depicted in this figure.

These ACMs also present wall thickness from 250 to 800 μm, hydraulic diameter from 0.7 to 4 cm, open frontal area between 5% and 25%, and geometric surface area from 0.7 to 1 cm^2/cm^3. Furthermore, the compression strength values of these ACMs ranged from 4.12 to 7.56 MPa, with the highest value being obtained for the Alcell lignin one [1].

As can be seen, the preparation method here exposed allowed for obtaining circular shaped ACMs with axial channels, at very low pressure (0.8 MPa), in contrast to monolithic discs that were reported in the literature, which were obtained at 130 MPa [2,3]. Furthermore, most of these ACMs reported in the literature were usually made by compressing the already reported activated carbon in the presence of a binder, obtaining the corresponding ACM in the form of solid discs [4–8]. However, these binding components can produce a significant reduction in the porosity of the resulting monolith.

Other authors proposed the preparation of ACMs by the extrusion of the impregnated material with different activating agents, in a similar way

to the one proposed in this work, but also with the goal of obtaining ACM discs [9–14]. In this sense, the preparation of ACMs with well-defined channels, like those here presented, was less reported and could be considered to be very useful for different applications.

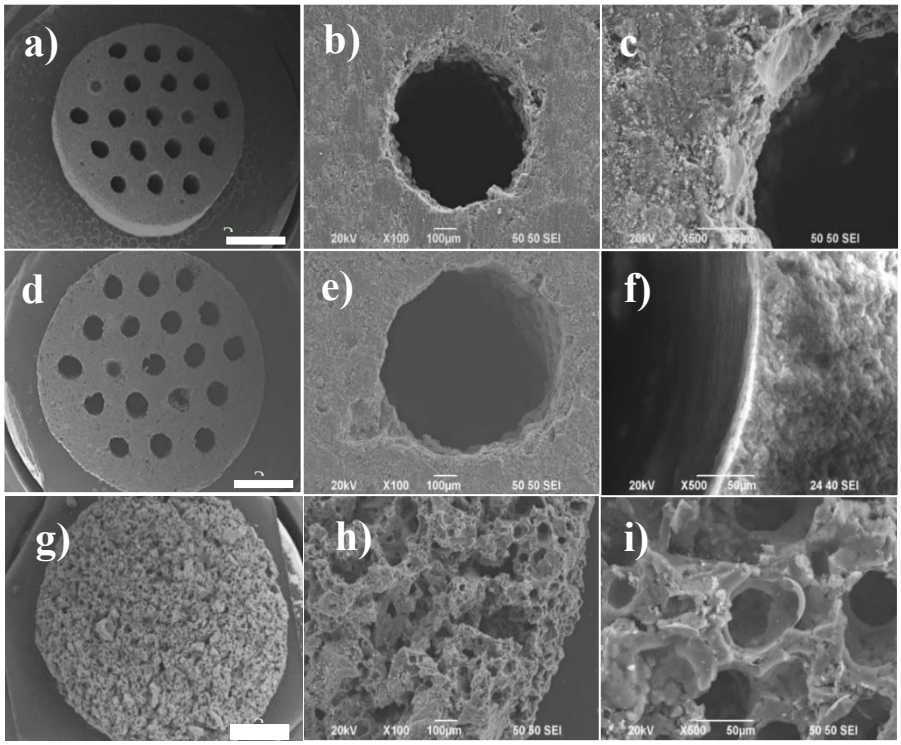

Figure 4.1. SEM micrographs of the activated carbon monoliths (ACMs) obtained from olive stone (a–c); Alcell lignin (d–f); and Kraft lignin (g–i), at an impregnation ratio of 1. Bar length of (a), (d), and (g) 2 mm.

Figure 4.2 collects a brief summary of some textural parameters for different ACMs that were derived from the N_2 adsorption-desorption

isotherms at −196 °C. The values of external surface area (A_t) were considerably lower than those for the apparent surface area (A_{BET}), which suggested that the main surface area is contained in micropores. The high values of A_{BET} that were found for the different ACMs, which ranged from 700 to 1500 m^2/g, also indicate the high development of the porosity that was obtained in these monoliths. Specifically, the highest values for these textural parameters were obtained for the ACM derived from olive stone and prepared at the impregnation ratio of 2. These values are in the same range than those that were reported for a powder activated carbon from olive stone prepared by chemical activation with phosphoric acid at an impregnation ratio of 1, and a temperature of 500 °C (A_{BET} ~900 m^2/g) [15], which suggests that the extrusion of the impregnated samples, followed by activation, does not limit the development of porosity, when compared to the traditional method that was carried out by the extrusion of a mixture of activated carbon with a binder. In any case, ACMs from both Alcell lignin and olive stone presented A_{BET} values that were higher than 1000 m^2/g; values that were quite remarkable for catalytic applications.

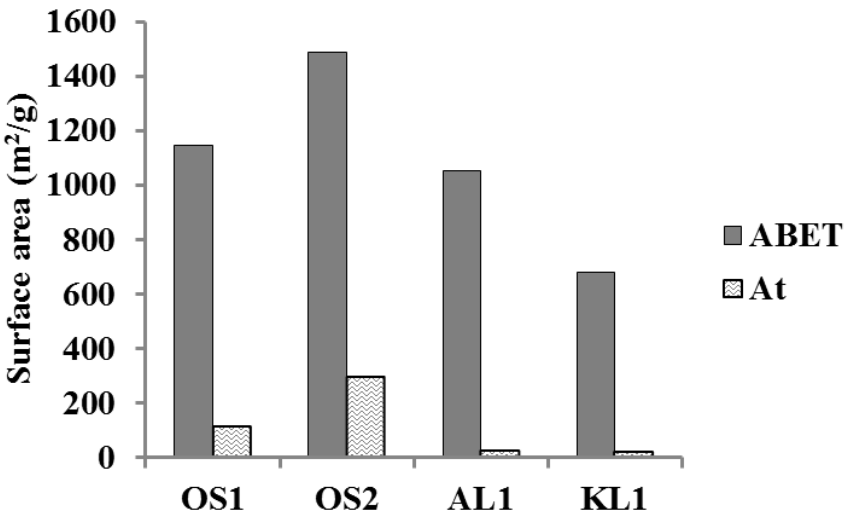

Figure 4.2. Comparison of the apparent surface area (A_{BET}) and external surface area (At) derived from N_2 adsorption-desorption data of the different ACMs.

Figure 4.3 shows the cumulative pore volume of the ACMs derived from both the N_2 adsorption at −196 °C by using two-dimensional-Non Localized Density Functional TheoryNLDFT (2D-NLDFT) heterogeneous adsorption models for carbon slit-shaped pores and Hg porosimetry. Specifically, a cumulative pore volume at different pore size intervals is represented for the different catalysts. As can be seen, OS2 and AL1 presented a very similar volume of micropores (pore sizes lower than 2 nm), but OS2 was the ACM with the largest contribution of pore size, between 0 and 10 nm (in the range of micropores and narrow mesopores). In the interval of pore size between 1×10^2 and 5×10^3 nm

(macropores), OS1 presented the highest pore volumes. On the other hand, OS2 showed the highest pore volume in the range of narrow mesoporosity, which is a consequence of the larger external surface area observed for this ACM (Figure 4.2).

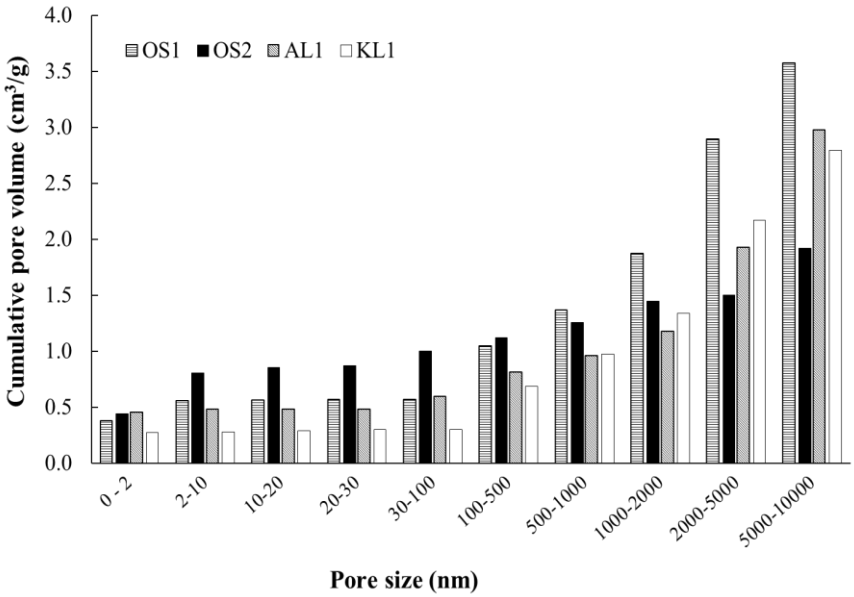

Figure 4.3. Cumulative pore volume of the ACMs catalysts derived from both the N_2 adsorption-desorption at −196 °C (micropore and mesopore range) and Hg porosimetry (macropore range).

Table 4.1 collects the mass surface concentration of phosphorus that was determined by XPS analyses. As can be seen, the phosphorus surface concentration values were found between 2.1 and 4.5%. The presence of phosphorus chemically stable on the surface of the ACMs is a well-known consequence of the activation method with phosphoric acid at

certain preparation conditions. This phosphorus remained on the ACM surface, even after the washing step, mainly in form of –C–O–PO_3 and –C–PO_3 species [16,17]. In this sense, KL1 showed the highest P surface concentration and also the largest contribution of the more oxidized phosphorus species [1]. The importance of this P content was mainly related to the fact that phosphates and polyphosphate esters that are found on the ACM surface had hydroxyl groups (–OH) that acted as Brönsted acid sites, giving up protons (H+) during the alcohol dehydration reaction [18]. Therefore, there should be a correlation between the amount of phosphorus that remains on the catalyst surface and the acidity of the ACMs.

Table 4.1. Mass surface concentration of phosphorus determined by X-ray photoelectron spectroscopy (XPS) analyses and CO and CO_2 evolved quantities from temperature-programmed desorption (TPD) experiments.

ACMs Catalysts	P_{XPS} (wt.%)	CO_{TPD} (mmol/g)	$CO_{2\ TPD}$ (mmol/g)
OS1	2.8	5.5	0.6
OS2	3.2	6.4	0.4
AL1	3.7	6.1	0.5
KL1	4.5	9.5	0.7

On the other hand, Bedia et al. analyzed the acidity of different powder activated carbons that were prepared by chemical activation with phosphoric acid by NH_3-TPD [15]. The total amount of ammonia desorbed showed a clear relationship with the amount of oxygen surface groups that decompose as CO and CO_2 during the TPD experiments, indicating the relevance of carrying this type of experiments in terms of acidity of the catalysts. Table 4.1 also summarizes the amount of CO and CO_2 that evolved from TPD experiments under inert flow. The amount of oxygen surface groups decomposing as CO was significantly higher for KL1, and very similar for AL1 and OS2. The presence of CO-evolving groups was also considerably greater than that of the CO_2-evolving groups, this latter being related to the small amounts of carboxyl, lactonic, and anhydride surface groups. The higher evolution of CO was mainly observed at temperatures higher than 700 °C and associated with the presence of the C–O–PO_3 groups that formed during the activation of lignocellulosic materials with phosphoric acid, which decomposed as CO at high temperatures (~860 °C) [16,17,19]. Valero-Romero et al. associated a weak and moderate-strength acidity to these C–O–P type species [20]. Therefore, there seems to be a close relationship between the specific amount of CO-evolving groups and the acidity of these ACMs.

Isopropyl Alcohol (IPA) decomposition was used to characterize the acidity of the ACMs. Figure 4.4 shows the steady-state conversions of IPA and the selectivity to dehydrogenation and/or dehydration products as a function of the reaction temperature for all of the ACMs (Po_{IPA} = 0.03 atm; W/Fo_{IPA} = 0.1 g·s/μmol). In general, the IPA conversion increased with the reaction temperature and OS2 showed higher catalytic activity than the other ACMs ones at any temperature.

The main reaction product was propylene that derived from the dehydration reaction. The selectivity to propylene was very high at all of the evaluated temperatures. Only small quantities of diisppropyl ether were observed at low temperatures and IPA conversions, showing a selectivity to propylene that was higher than 90% for temperatures higher than 250 °C, for all the ACMs. These results suggested that these ACMs developed a relatively large amount of surface acidity during the preparation procedure and, thus, there would be no need for additional treatments to increase the acidity of these catalysts, such as activated carbon oxidation with nitric acid [21].

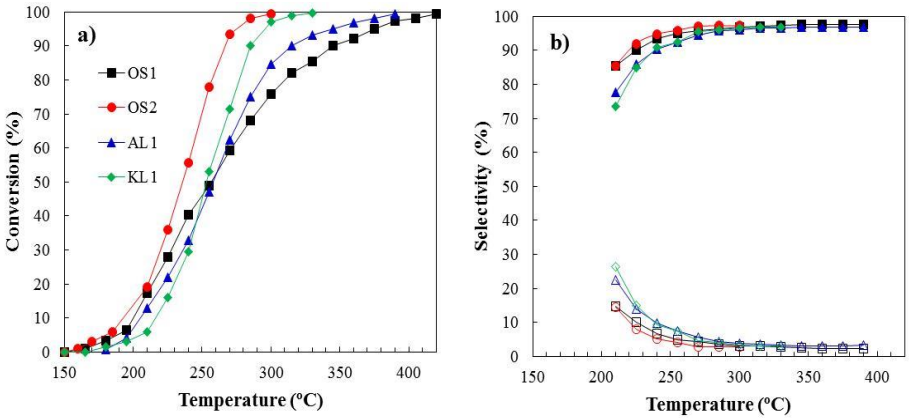

Figure 4.4. (a) IPA steady state conversion and (b) selectivity to propylene (filled marks) and diisoppropyl ether (hollow marks) as a function of the reaction temperature for the different carbon monoliths catalysts under inert atmosphere. P_{0IPA} = 0.03 atm; W/F_{0IPA} = 0.1 g·s/µmol.

Mass transport limitations can be neglected based on the theoretical calculations of Carberry number and the isothermal intraphase internal effectiveness factor, at the operating conditions that were used in this study [20]. The values of apparent rate constant, k, have been obtained using conversion values below 20%, taken into account a global first-order kinetic. From these values and applying the Arrhenius equation, the corresponding values of apparent activation energy (Ea) and the preexponential factor (A) have been calculated for each ACM and they are summarized in Table 4.2. The values that were obtained for the apparent activation energies were quite similar, ranging from 100 to 130

kJ/mol and of the same order than those that were obtained for different inorganic catalysts (heteropolyacids, zeolites,…) [22,23] and powder activated carbons that were obtained by chemical activation with phosphoric acid from different lignocellulosic waste [15,24].

Table 4.2. Apparent kinetic parameters for 2-propanol decomposition for all the ACM catalysts.

	Ea (kJ/mol)	ln k_o
OS1	104	33.14
OS2	116	36.34
AL1	134	39.70
KL1	136	50.99

Preexponential factor values can provide a rough estimation of the amount of active sites per unit of surface area or unit of mass of catalyst. As can be seen, the values that were reported in Table 4.2 followed the same sequence than the P content that was determined by XPS (see Table 2), KL1 > AL1 > OS2 > OS1, which suggested that the number of active sites are directly related to the presence of phosphates and polyphosphate esters in the different ACMs. A relationship between the amount of

surface phosphorus complexes (of C–O–P type) and surface acidity has been also reported [25].

4.2. Methanol Decomposition

Once the acidity of the ACMs was evidenced, these catalysts were used for the methanol dehydration reaction. The catalytic activity of the ACMs here reported are denoted in Figure 4.5, where the methanol conversion, $X_{MeOH,}$ as a function of the reaction temperature was represented. The reaction of methanol dehydration was carried out in the presence of air (P_{MeOH} = 0.03 atm, W/F_{MeOH} = 0.01 g·s/µmol). A temperature of 375 °C was selected as the maximum reaction temperature that the carbon monoliths can stand without the significant gasification of the carbonaceous matrix. These carbon-based catalysts could work at such a high temperature without burning out due to the high oxidation resistance that was provided by the presence of these P surface complexes [1]. The highest conversion obtained was approximately 70% at 375 °C, with OS2 being the most active ACM due to its higher value of apparent surface area, which compensates its slightly lower P content. The rest of ACMs follows the sequence OS1>KL1>AL1.

DME was the main reaction product. The selectivity to this product was higher than 90% for all the ACMs up to 350 °C. At 375 °C, the selectivity to DME decreased to around 85% due to the appearance of CO2 and, in less extent CO in the outlet stream. The burn-off of the ACMs was considerable at higher temperatures and the methanol dehydration was not evaluated. Other authors have evaluated different activated carbons as catalysts for the methanol dehydration reaction, and they have reported much lower methanol conversions, although under inert atmosphere [26, 27]. The P surface complexes C-O-P type play an important role for an efficient and highly selective methanol dehydration to DME, given that they present a weak-to-moderate acid strength [24,28] and provide the carbon surface with high oxidation resistance [19,25]. In a previous work, we had reported that these P surface groups would seem to be the active sites that are responsible for the relatively high conversion of methanol to DME [20]. These active sites had presented a redox function, avoiding (in the presence of air) the catalyst deactivation by coke deposition due to a continuous (re)oxidation of the reduced P surface groups, which are produced by the dehydration reaction, without a significant the burn-off of the carbon matrix of the catalyst.

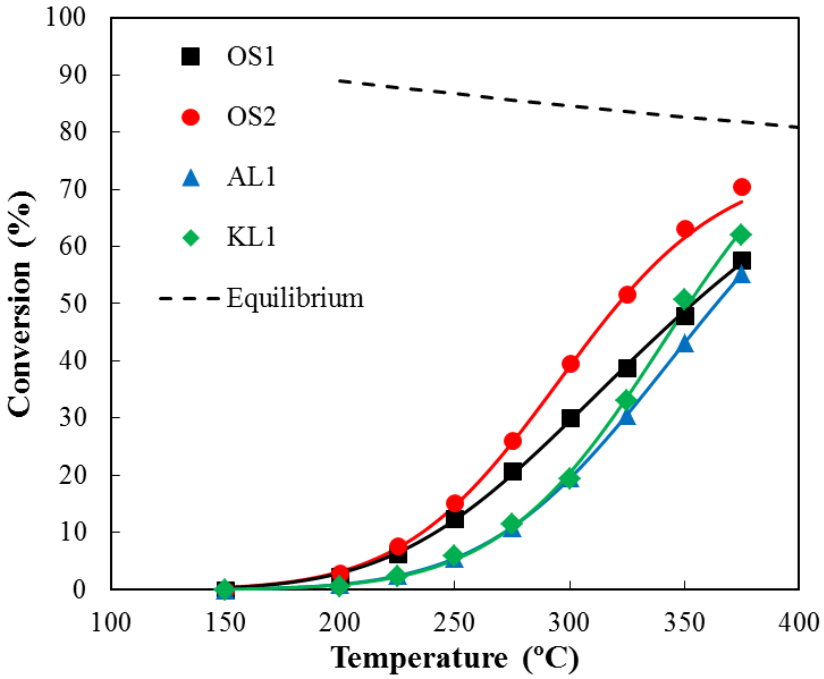

Figure 4.5. Methanol conversion as a function of the reaction temperature for the different carbon monoliths catalysts under air conditions. P_{MeOH} = 0.03 atm, W/F_{MeOH} = 0.1 g·s/µmol. Dots: experimental data, lines: Langmuir-Hinshelwood model fitting; dash lines: equilibrium conversions.

4.2.1. Stability Study

With the goal of studying the stability of OS2 monolith under reaction, a long-term experiment was carried out at two different temperatures. Figure 4.6 shows DME yields as a function of the time on stream at 300 and 350 °C, at P_{MeOH} = 0.03 atm and W/F_{MeOH} = 0.1 g·s/µmol. Almost no decrease of the DME yield was observed at 300 °C for 20 h of time

on stream, which evidenced the high stability of this catalyst under these operating conditions. At 350 °C, a gradual decrease of the methanol conversion could be observed, which was mainly related to a progressive deactivation of the catalyst by coke deposition. However, it is important to point out that methanol conversions higher than 45% have been obtained for more than 20 h, with selectivity towards DME practically the same, with values higher than 85%.

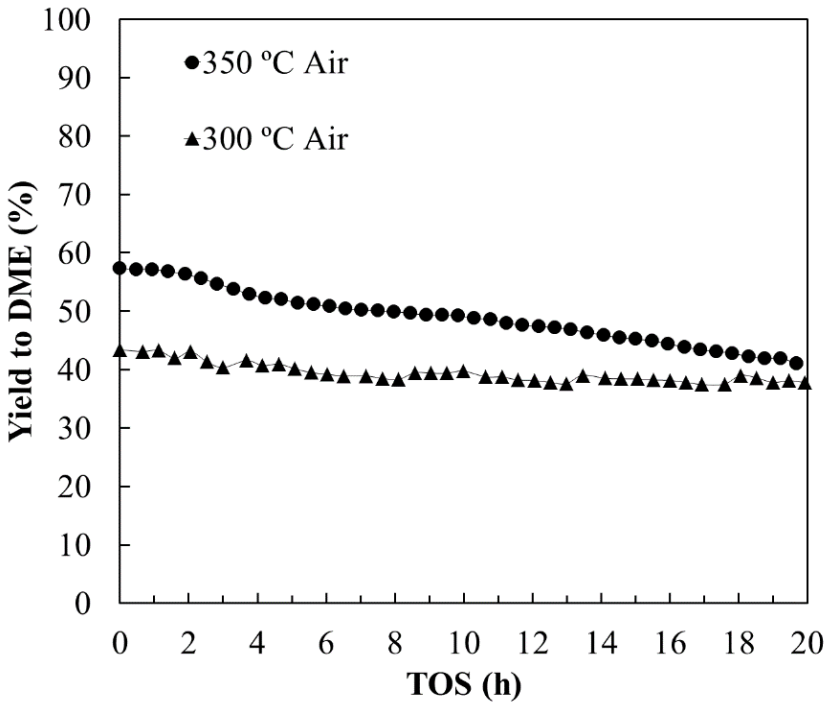

Figure 4.6. DME yield as a function of the time on stream at different reaction temperatures for OS2 monolith under air atmosphere. P_{MeOH} = 0.03 atm, W/F_{MeOH} = 0.1 g·s/µmol.

4.2.2. Influence of Water Vapor in the Reaction Mixture

The methanol dehydration reaction to DME can be significantly influenced by the presence of water vapor, which may shift the reaction equilibrium [29, 30]. The influence of the presence of water in the methanol conversion was analyzed for OS2. Figure 4.7 shows the methanol steady state conversion for different inlet partial pressures of water at 300 and 350 °C in air. For the sake of comparison, methanol equilibrium conversions were also included in the dash lines. Methanol conversions significantly decreased in the presence of water, as compared to the equilibrium conversions, which was due to its competitive adsorption with methanol for the acid sites. Specifically, methanol conversion was reduced by half in the presence of 0.08 atm of water vapor at 350 °C, meanwhile a decrease of almost 70% was observed at 300 °C, which indicated that the influence of water was less pronounced with the increase of reaction temperature, which was probably due to the adsorption enthalpy of water being slightly higher than that of methanol, according to the values that were reported in the literature [31,32]. DME formation also decreased from 99 to 86% in the presence of 0.08 atm of water, at 300 °C.

Valero-Romero et al. reported a methanol conversion decrease from 20 to 11% when the water content in the feed was raised to 0.04 atm at 300

°C, for a powder activated carbon [20]. This decrease was less pronounced than the one that was observed for OS2, in spite of both the powder activated carbon and the monolith (OS2) presenting very similar P contents, derived from XPS analyses. However, the experimental conditions for these two cases were slightly different. The inlet methanol concentration was lower for the case of the powder activated carbon, which would suppose a lower formation of water by the reaction and, therefore, a lower competitive adsorption between methanol and water vapor.

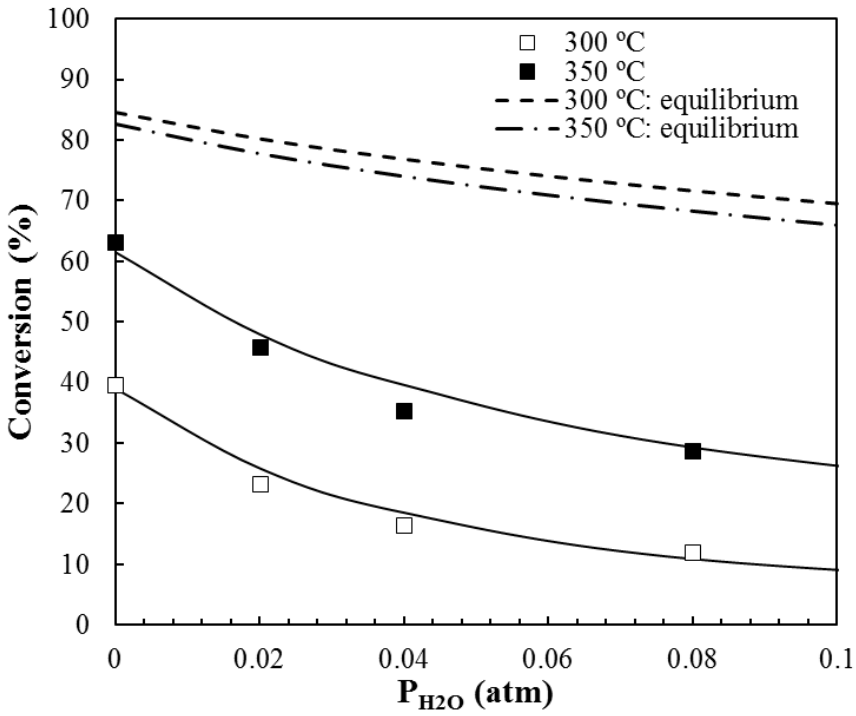

Figure 4.7. Methanol conversion as a function of different water partial pressures at 300 and 350ºC for OS2 monolith. P_{MeOH} = 0.03 atm, W/F_{MeOH} = 0.1 g·s/µmol. Dots: experimental data, lines: Langmuir-Hinshelwood model fitting; dash lines: methanol equilibrium conversions.

4.3. Kinetic Study

The steady-state catalytic methanol conversion data that were obtained at different temperatures were fitted using several kinetic models for an integral reactor. The reactor mass balance equation of the reactor was numerically integrated to calculate the methanol conversion.

$$X = \int_0^{\frac{W}{F_{MeOH}{}^0}} -r_{MeOH} \cdot d(\frac{W}{F_{MeOH}}) \qquad (1)$$

In this equation, $-r_{MeOH}$ represented the methanol decomposition rate, while $\frac{W}{F_{MeOH}{}^0}$ stood for the methanol space time (g·s/µmol).

The mathematical description of $-r_{MeOH}$ relied on the kinetic mechanism for methanol decomposition over acid catalysts. It has been supposed that methanol dehydration was the prevailing reaction contributing to $-r_{MeOH}$ since selectivity towards dimethyl ether was higher than 90% for most of the experiments. Two different reaction pathways for this reaction were proposed, which involved the associative and dissociative mechanisms [33]. The dissociative mechanism, the most generally accepted, considers that an intermediate methoxyl is formed on the acid site after the adsorption of a methanol molecule [34]. A nucleophilic attack by a second methanol molecule results in the dimethyl ether formation, releasing water as a by-product. In addition, the competitive adsorption of water on the active sites is responsible for a decrease in the catalytic activity. Oxygen is not included in the main reaction pathway, and its role is ascribed to the oxidation of the intermediates that would deliver catalyst deactivation through the formation of light hydrocarbons and coke.

From these considerations, three kinetic models were proposed to describe the methanol decomposition rate: i) Pseudo-second order (SO) with respect to methanol concentration, ii) Langmuir-Hinshelwood (LH) mechanism, and iii) Eley-Rideal mechanism (ER). The resulting kinetic rate expressions are collected in Table 4.3. The LH and ER mechanisms also include the competitive adsorption of water. It must be noted that the relationship of the kinetic and equilibrium constants, methanol adsorption constant, and water adsorption constant (denoted as ksr, Ksr, K_{MeOH}, and K_{H2O}, respectively) with temperature are described while using Arrhenius and Van't Hoff laws:

$$k = k_0 \cdot e^{-\frac{Ea}{R \cdot T}} \qquad (2)$$

$$K_i = K_{0,i} \cdot e^{-\frac{\Delta H_i}{R \cdot T}} \qquad (3)$$

After selecting the appropriate rate expression, Equation (1) is numerically solved while using an ordinary differential equation solver. The related kinetic and adsorption parameters from Equations (2) and (3) are optimized by minimizing the objective function (OF), which is selected to be the sum of the quadratic difference between the experimental and modelled conversion data divided by the number of experimental data points. The optimization is performed while using a

simplex search method. The integration and optimization of the models has been implemented using Matlab ®.

Table 4.3. kinetic rate expressions for the methanol decomposition.

Model	Rate Expression	OF Values
SO	$-r_{MeOH} = k \cdot {P_{MeOH}}^2$	3.387×10^{-3}
ER	$-r_{MeOH} = \dfrac{k_{SR} \cdot (K_{MeOH} \cdot {P_{MeOH}}^2 - \frac{P_{DME} \cdot K_{H2O} \cdot P_{H2O}}{K_{SR}})}{1 + K_{MeOH} \cdot P_{MeOH} + K_{H2O} \cdot P_{H2O}}$	1.025×10^{-3}
LH	$-r_{MeOH} = \dfrac{k \cdot (K_{MeOH} \cdot {P_{MeOH}}^2 - \frac{P_{DME} \cdot K_{H2O} \cdot P_{H2O}}{K_{SR}})}{(1 + K_{MeOH} \cdot P_{MeOH} + K_{H2O} \cdot P_{H2O})^2}$	0.961×10^{-3}

The optimization results reveal that SO is not able to fairly reproduce the experimental data (OF value three times higher than LH and ER ones, Table 4.3). Mechanisms considering surface reaction on the active site, such as the ER and LH models, are required in providing an accurate mathematical description of the methanol conversion dependence with temperature on these catalysts. The most probable model seems to be LH, according to the lower value that was obtained for the OF (Table 4.3), although further experiments at higher methanol pressures would be necessary to confirm this finding.

The modeled data (solid lines) calculated from the optimized LH kinetic and adsorption parameters assuming the integral reactor equation have been also included in Figure 4.5, showing an excellent agreement. The LH model could describe the impact of the presence of water in the reactor feed on the methanol conversion very well. In this sense, the LH mechanism with competitive water adsorption provides the best model predictions for the methanol conversion in OS2 monolith when different amounts of steam were added to the reactor inlet at 300 and 350 °C (see Figure 4.7).

Table 4.4 compiles the values of the LH model parameters. The activation energies that were obtained are in accordance to those previously found for other acid activated carbon catalysts used for methanol dehydration and even, for other inorganic materials [27, 35, 36]. The most active monolith, OS2, showed the lowest activation energy value. Moreover, the evaluation of the kinetic and adsorption constant at 300 °C (the two last columns on Table 4.4) revealed that the kinetic constant value followed the order OS1 > AL1 > OS2~KL1, whereas the adsorption constant showed a quite different trend, OS2>KL1~OS1>AL1. The combination of both constant values can explain the higher methanol conversion that was attained at low temperature by the OS1 and OS2 monolith. On the other hand, the lower

affinity of OS1 surface for methanol would explain why OS2 outperforms OS1 as the reaction temperature increased. The evaluation of K_{H2O} value at 300 °C ($K_{H2O,300}$ = 15.8 atm^{-1}) revealed that the affinity of the OS2 surface towards water was higher than that for methanol at those conditions. Therefore, the addition of water to the inlet gas could effectively displace methanol from the adsorption sites when its pressure was high enough, a fact that could be behind the activity drop that was observed for OS2 in the presence of water vapor (Figure 4.7).

Table 4.4. Langmuir-Hinshelwood (LH) Model parameter values.

Sample	$10^{-5}\cdot k_{0,SR}$ mol $s^{-1}g^{-1}$	Ea_{SR} kJ mol^{-1}	$K_{0,SR}$	ΔH_{SR} kJ mol^{-1}	K_0^{MeOH} atm^{-1}	ΔH^{MeOH} kJ mol^{-1}	K_0^{H2O} atm^{-1}	ΔH^{H2O} kJ mol^{-1}	$10^5\cdot k_{SR,300}$ mol s^{-1} g^{-1}	$K_{MeOH,300}$ atm^{-1}
AL1	49	99	12	21	0.037	−15	0.007	−26	395	0.8
KL1	354	111	43	24	0.025	−18	0.003	−17	269	1.1
OS1	24	96	29	27	0.027	−17	0.011	−33	445	1.1
OS2	6.2	92	19	25	0.155	−12	0.009	−35	276	1.8

4.4. Conclusions

Activated carbon monoliths (ACMs) from different lignocellulosic biomass waste, such as olive stone (OS), Alcell (AL), and Kraft lignin (KL), were prepared by the direct extrusion of the precursors with phosphoric acid, followed by activation under inert atmosphere, and washing with distilled water. These activated carbon monoliths were used as catalysts for the alcohol dehydration reaction. The highest conversion for Isopropyl Alcohol decomposition was obtained by the ACMs that were derived from olive stone. Selectivity to propylene was quite high at all of the evaluated temperatures, being higher than 90% from 250 °C, for all the ACMs. The values for the apparent activation energies (supposing a first-order kinetic) are quite similar, ranging from 100 to 130 KJ/mol.

The methanol decomposition reaction was also analyzed under air atmosphere. The highest conversion obtained, without a significant burn-off of the carbonaceous matrix, is approximately 70% at 375 °C, with OS2 being the most active ACM, followed by KL1 and AL1 catalyst. Several kinetic models were evaluated to predict the methanol conversions, while taking also into account the competitive influence of water. The Langmuir-Hinshelwood mechanism, whose rate-limiting step was the surface reaction between two adsorbed methanol molecules,

represented the experimental data under the conditions studied very well. An activation energy value of 92 kJ/mol for methanol dehydration reaction and adsorption enthalpies for methanol and water of −12 and −35 kJ/mol, respectively, were obtained.

4.5 References

[1] Ibeh, P.O.; García-Mateos, F.J.; Rosas, J.M.; Rodríguez-Mirasol, J.; Cordero, T. Activated carbon monoliths from lignocellulosic biomass waste for electrochemical applications. *J. Taiwan Inst. Chem. Eng.* **2019**, *97*, 480–488.

[2] Molina-Sabio, M.; Rodríguez-Reinoso, F.; Caturla, F.; Sellés, M.J. Porosity in granular carbons activated with phosphoric acid. *Carbon* **1995**, *33*, 1105–1113.

[3] Nakagawa, Y.; Molina-Sabio, M.; Rodríguez-Reinoso, F. Modification of the porous structure along the preparation of activated carbon monoliths with H_3PO_4 and $ZnCl_2$. *Micropor. Mesopor. Mater.* **2007**, *103*, 29– 34.

[4] Lozano-Castelló, D.; Cazorla-Amorós, D.; Linares-Solano, A.; Quinn, D.F. Activated carbon monoliths for methane storage: Influence of binder. *Carbon* **2002**, *40*, 2817–2825.

[5] Lim, J.W.; Choi, Y.; Yoon, H.S.; Park, Y.K.; Yim, J.H.; Jeon, J.K. Extrusion of honeycomb monoliths employed with activated carbon-LDPE hybrid materials. *J. Ind. Eng. Chem.* **2010**, *16*, 51–56.

[6] Liu, L.; Liu, Z.; Yang, J.; Huang, Z.; Liu, Z. Effect of preparation conditions on the properties of a coal-derived activated carbon honeycomb monolith. *Carbon* **2007**, *45*, 2836–2842.

[7] Machnikowski, J.; Kierzek, K.; Lis, K.; Machnikowska, H.; Czepirski, L. Tailoring Porosity Development in Monolithic Adsorbents Made of KOH-Activated Pitch Coke and Furfuryl Alcohol Binder for Methane Storage. *Energ. Fuel.* **2010**, *24*, 3410–3414.

[8] Jordá-Beneyto, M.; Lozano-Castelló, D.; Suárez-García, F.; Cazorla-Amorós, D.; Linares-Solano, Á. Advanced activated carbon monoliths and activated carbons for hydrogen storage. *Micropor. Mesopor. Mater.* **2008**, *112*, 235–242.

[9] Paola Vargas, D.; Giraldo, L.; Silvestre-Albero, J.; Moreno-Piraján, J.C. CO_2 adsorption on binderless activated carbon monoliths. *Adsorption* **2011**, *17*, 497–504. *Materials* **2019**, *12*, 2394 14 of 14

[10] Vargas, D.D.P.; Giraldo, G.L.; Moreno, P.J.C. Enthalpic characterisation of activated carbon monoliths obtained from lignocellulosic materials. *J. Therm. Anal. Calorim.* **2013**, *111*, 1067–1072.

[11] García-Blanco, A.A.; Oliveira, J.C.A. De; López, R.; Moreno-piraján, J.C.; Giraldo, L.; Zgrablich, G.; Sapag, K. A study of the pore size distribution for activated carbon monoliths and their relationship

with the storage of methane and hydrogen. *Colloids Surfaces A Physicochem. Eng. Asp.* **2010**, *357*, 74–83.

[12] Djeridi, W.; Ouederni, A.; Wiersum, A.D.; Llewellyn, P.L.; Mir, L. El High pressure methane adsorption on microporous carbon monoliths prepared by olives stones. *Mater. Lett.* **2013**, *99*, 184–187.

[13] Taer, E.; Deraman, M.; Taslim, R.; Iwantono. Preparation of Binderless Activated Carbon Monolith from Pre-Carbonization Rubber Wood Sawdust by Controlling of Carbonization and Activation Condition. *AIPConf. Proc.* **2013**, *1554*, 33–37.

[14] Ubago-Pérez, R.; Carrasco-Marín, F.; Fairén-Jiménez, D.; Moreno-Castilla, C. Granular and monolithic activated carbons from KOH-activation of olive stones. *Micropor. Mesopor. Mater.* **2006**, *92*, 64–70.

[15] Bedia, J.; Rosas, J.M.; Márquez, J.; Rodríguez-Mirasol, J.; Cordero, T. Preparation and characterization of carbon based acid catalysts for the dehydration of 2-propanol. *Carbon* **2009**, *47*, 286–294.

[16] Rosas, J.M.; Bedia, J.; Rodríguez-Mirasol, J.; Cordero, T. Preparation of hemp-derived activated carbon monoliths. Adsorption of water vapor. *Ind. Eng. Chem. Res.* **2008**, *47*, 1288–1296.

[17] Rosas, J.M.; Bedia, J.; Rodríguez-Mirasol, J.; Cordero, T. HEMP-derived activated carbon fibers by chemical activation with phosphoric acid. *Fuel* **2009**, *88*, 19–26.

[18] Bedia, J.; Rosas, J.M.; Vera, D.; Rodríguez-Mirasol, J.; Cordero, T. Isopropanol decomposition on carbon based acid and basic catalysts. *Catal. Today* **2010**, *158*, 89–96.

[19] Rosas, J.M.; Ruiz-Rosas, R.; Rodríguez-Mirasol, J.; Cordero, T. Kinetic study of the oxidation resistance of phosphorus-containing activated carbons. *Carbon* **2012**, *50*, 1523–1537.

[20] Valero-Romero, M.J.; Calvo-Muñoz, E.M.; Ruiz-Rosas, R.; Rodríguez-Mirasol, J.; Cordero, T. Phosphorus-Containing Mesoporous Carbon Acid Catalyst for Methanol Dehydration to Dimethyl Ether. *Ind. Eng. Chem. Res.* **2019**, *58*, 4042–4053.

[21] Carrasco-Marín, F.; Mueden, A.; Moreno-Castilla, C. Surface-Treated Activated Carbons as Catalysts for the Dehydration and Dehydrogenation Reactions of Ethanol. *J. Phys. Chem. B* **1998**, *102*, 9239–9244.

[22] Turek, W.; Haber, J.; Krowiak, A. Dehydration of isopropyl alcohol used as an indicator of the type and strength of catalyst acid centres. *Appl. Surf. Sci.* **2005**, *252*, 823–827.

[23] Trens, P.; Stathopoulos, V.; Hudson, M.J.; Pomonis, P. Synthesis and characterization of packed mesoporous tungsteno-silicates: application to the catalytic dehydrogenation of 2-propanol. *Appl. Catal. A Gen.* **2004**, *263*, 103–108.

[24] Bedia, J.; Ruiz-Rosas, R.; Rodríguez-Mirasol, J.; Cordero, T. A kinetic study of 2-propanol dehydration on carbon acid catalysts. *J. Catal.* **2010**, *271*, 33–42.

[25] Valero-Romero, M.J.; García-Mateos, F.J.; Rodríguez-Mirasol, J.; Cordero, T. Role of surface phosphorus complexes on the oxidation of porous carbons. *Fuel Process. Technol.* **2017**, *157*, 116–126.

[26] Jasiñska, J.; Krzyžyñska, B.; Kozłowski, M. Influence of activated carbon modifications on their catalytic activity in methanol and ethanol conversion reactions. *Cent. Eur. J. Chem.* **2011**, *9*, 925–931.

[27] Moreno-Castilla, C.; Carrasco-Marín, F.; Parejo-Pérez, C.; López Ramón, M. Dehydration of methanol to dimethyl ether catalyzed by oxidized activated carbons with varying surface acidic character. *Carbon* **2001**, *39*, 869–875. *Materials* **2019**, *12*, 2394 13 of 14

[28] Bedia, J.; Barrionuevo, R.; Rodríguez-Mirasol, J.; Cordero, T. Ethanol dehydration to ethylene on acid carbon catalysts. *Appl. Catal. B Environ.* **2011**, *103*, 302–310.

[29] Vishwanathan, V.; Roh, H.; Kim, J.; Jun, K. Surface properties and catalytic activity of TiO_2–ZrO_2 mixed oxides in dehydration of methanol to dimethyl ether. *Catal. Lett.* **2004**, *96*, 23–28.

[30] Mollavali, M.; Yaripour, F.; Atashi, H.; Sahebdelfar, S. Intrinsic Kinetics Study of Dimethyl Ether Synthesis from Methanol on γ-Al_2O_3 Catalysts. *Ind. Eng. Chem. Res*. **2008**, *467*, 3265–3273.

[31] Sierra, I.; Ereña, J.; Aguayo, A.T.; Ateka, A.; Bilbao, J. Kinetic Modelling for the Dehydration of Methanol to Dimethyl Ether over γ-Al_2O_3. *Chem. Eng. Trans.* **2013**, *32*, 613–618.

[32] Kasaie, M.; Sohrabi, M. Kinetic Study on Methanol Dehydration to Dimethyl Ether Applying Clinoptilolite Zeolite as the Reaction Catalyst. *J. Mex. Chem. Soc.* **2009**, *53*, 233–238.

[33] Sun, J.; Yang, G.; Yoneyama, Y.; Tsubaki, N. Catalysis Chemistry of Dimethyl Ether Synthesis. *ACS Catal.* **2014**, *4*, 3346–3356.

[34] Chang, C.D. *Mechanism of Hydrocarbon Formation from Methanol.* Studies in Surface Science and Catalysis. Elsevier: *Amsterdam, The* Nederland, 1988; Volume 36, pp. 127–143.

[35] Aguayo, T.; Gayubo, A.G.; Vivanco, R.; Olazar, M.; Bilbao, J. Role of acidity and microporous structure in alternative catalysts for the transformation of methanol into olefins. *Appl. Catal. A Gen.* **2005**, *283*, 197–207.

[36] Ruiz-Rosas, R.; Bedia, J.; Rosas, J.M.; Lallave, M.; Loscertales, I.G.; Rodríguez-Mirasol, J.; Cordero, T. Methanol decomposition on electrospun zirconia nanofibers. *Catal. Today* **2012**, *187*, 77–87.

RESUMEN

El objetivo de esta tesis es la preparación de monolitos de carbón activado (ACMs) sin la necesidad de añadir ningún tipo de aglutinante a partir de diferentes residuos biomásicos, como la lignina y huesos de aceituna. El primer residuo es en realidad un subproducto de la industria papelera y, también podría obtenerse en las biorrefinerías lignocelulósicas destinadas a la producción de bioetanol y el segundo residuo usado procede de la industria olivarera. Concretamente se han usado la lignina Kraft y Alcell® y los huesos de aceituna, los cuales son impregnados con H_3PO_4, se extruyen en diferentes conformaciones (discos y monolitos con diferente cantidad de canales) y, posteriormente, se activan. Para minimizar la posible fusión e hinchamiento de la lignina durante la etapa de activación, se han probado diferentes metodologías. Además, las propiedades electroquímicas de los ACMs han sido analizadas.

Por otro lado, estos ACMs también se evaluaron como catalizadores para la producción de dimetil éter (DME). La actividad y la estabilidad de estos ACMs en la reacción de deshidratación del metanol se analizaron en una atmósfera de aire. También se estudió la influencia de la presencia de agua la corriente de alimentación para la deshidratación del metanol.

Finalmente se propuso un modelo cinético que fuera capaz de reproducir los resultados experimentales.

Preparación de ACM

Los ACMs se prepararon a partir de diferentes precursores de biomasa: lignina Alcell® (AL) (Repap Technologies Inc.), lignina de eucalipto obtenida a partir del proceso Kraft (KL) y hueso de aceituna (OS) suministrado por S.C.A. Olivarera y Frutera San Isidro, Periana (Málaga). Las materias primas fueron molidas y tamizadas hasta un intervalo de tamaño de partícula de 50-80 µm.

Estos precursores biomásicos se impregnaron con H_3PO_4 en una relación de impregnación de 1 (masa de H_3PO_4/masa de materia prima) y se mantuvieron en una estufa a vacío durante 24 horas, a 60 ºC.

Para estudiar el efecto de la relación de impregnación, también se impregnó hueso de aceituna con relaciones de impregnación de 1 y 2. Las muestras secas e impregnadas se mezclaron con agua destilada hasta obtener las propiedades reológicas y de plasticidad adecuadas para permitir su extrusión. Así, las muestras impregnadas, sin ningún tipo de aglomerante, fueron extruidas en una extrusora diseñada por nuestro grupo de investigación, utilizando un molde cilíndrico con un diámetro interno de 2 cm a temperatura ambiente y con una presión de 0,8 MPa.

La extrusora consta principalmente de un molde cilíndrico de acero inoxidable con un diámetro interno de 2 cm, y diferentes elementos de matriz (diámetro interno de 1 cm), operados a temperatura ambiente. El montaje es capaz de proporcionar un máximo de 1,6 MPa, aunque en la preparación de estos ACM, la presión no ha superado, en ningún caso los 0,8 MPa. También se diseñaron dos elementos de matriz diferentes con 19 y 72 pines para obtener monolitos con 25 y 120 canales/cm^2, respectivamente.

Cuando se utilizaron ambas ligninas como materia prima, fue necesario un paso de estabilización de las muestras impregnadas, previo a la extrusión, para evitar parcialmente los problemas de hinchamiento que presenta típicamente la lignina. Los métodos optimizados consisten en un tratamiento térmico a 250 ºC, bajo un flujo de aire (150 cm^3/min), durante 1 h. Luego, el 50% del material estabilizado se molió y se mezcló con un 50% de lignina impregnada no estabilizada, obteniendo una pasta que finalmente se extruyó para formar los monolitos.

Posteriormente, los monolitos obtenidos se activaron en un horno tubular a 700 ºC durante 2 h, con una velocidad de calentamiento de 10 ºC/min, bajo un flujo de nitrógeno. Finalmente, los monolitos activados se lavaron con agua destilada a 60 ºC, hasta obtener un pH constante en las aguas de lavado.

Caracterización de los ACMs

Para la caracterización de los ACMs se realizaron inicialmente análisis termogravimétricos (TGA) no isotermos de los diferentes precursores biomásicos (lignina y hueso de aceituna) bajo atmósfera de aire en una termobalanza, CI Electronics. La termobalanza mide automáticamente el peso de la muestra y la temperatura en función del tiempo. Los experimentos se llevaron a cabo con un caudal total de 150 mL (STP)/min, empleando una masa de muestra de aproximadamente 10 mg. A partir de estos ensayos se obtuvo el análisis inmediato de los precursores, donde se obtuvo que la lignina Kraft era el precursor con un mayor contenido en cenizas (KL-12,4%> AL -0,1%> OS-0,1%). Por otro lado, el análisis elemental de las muestras se realizó utilizando un analizador LECO CHNS 932, donde el contenido de oxígeno correspondiente se calculó por diferencia. Los resultados mostraron que la lignina Alcell era la que mostraba el mayor porcentaje de contenido en carbono en comparación con los otros precursores (AL 65%> KL 58%> OS 48%), el contenido de hidrógeno fue casi el mismo con un promedio de 6,6%, mientras que el contenido de oxígeno es indirectamente proporcional al contenido de carbono (AL 29% <KL 34% <OS 44%). Además, no se observaron rastros de azufre (S) en las

muestras AL y OS. En el caso de KL, el significativamente alto porcentaje de azufre deriva de su procedimiento de obtención.

La morfología de los ACMs (OS1, AL1, KL1) fue analizada mediante microscopía electrónica de barrido (SEM), con un analizador JEOL JSM-6490LV, obtenido a un voltaje de entre 20–25 kV. Las micrografías obtenidas demostraban la posibilidad de formar discos de carbón activo y de igual tamaño, a partir de diferentes precursores biomásicos, mediante una técnica sencilla y versátil. Es importante mencionar que los ACMs obtenidos a partir de la lignina necesitaban un tratamiento de estabilización previo para evitar el hinchamiento de la misma durante la etapa de activación. A partir de los resultados obtenidos, se pudo observar que los monolitos obtenidos a partir de OS y AL eran bastante similares, mientras que el obtenido a partir de lignina Kraft tenía una apariencia similar a un xerogel poroso. Además, para los monolitos de lignina de Alcell se compararon (a) los discos de carbono (b) los monolitos con 25 canales/cm^2 y (c) los monolitos con 120 canales/cm^2 obtenidos a una presión de 0,8 MPa. En las micrografías se observaban claramente los canales, incluso en aquel con una mayor densidad de huecos, bien alineados y distribuidos, lo que demostraba que con una extrusora de laboratorio, diseñada por nuestro grupo de investigación, era posible obtener, tanto discos, como monolitos con 25 y 120

canales/cm^2 a una relativamente baja presión. A diferencia de los previamente publicados en la bibliografía que se obtienen a presiones a partir de 130 MPa.

Es importante destacar que los ACMs pasan por una contracción de sus tamaños después de la etapa de activación. Por ejemplo, el diámetro de sección transversal de los monolitos OS y AL obtenidos a la misma relación de impregnación (1), se reduce aproximadamente un 25%. En general, se puede observar que los canales de ambos ACMs presentaban huecos circulares bastante regulares a lo largo de todo el monolito, con tamaños de canal que van desde 700 a 800 µm, mientras que la densidad de la celda de los diferentes ACMs varía entre 30 y 125 celdas / cm^2.

El rendimiento final de preparación de los diferentes ACMs fue calculado, presentando valores entre el 30 y el 40% (AL1= 41%> OS1= 40%> KL1= 32%). Estos valores están relacionados con la composición de la materia prima, es decir, el contenido de hemicelulosa, celulosa y lignina. Se observó que el monolito AL1 presentó un mayor rendimiento que los otros, debido a su mayor contenido en lignina y su baja cantidad de cenizas. En general, el rendimiento de los monolitos obtenidos a partir de hueso de aceituna disminuye con la relación de impregnación, como consecuencia de una deshidratación más profunda de la estructura carbonosa del precursor, por lo que el monolito, OS2, obtenido a una

relación de impregnación más alta (2), produjo un menor rendimiento en comparación con el OS1.

La textura porosa de los ACMs se evaluó mediante adsorción-desorción de N_2 a -196 ºC y adsorción de CO_2 a 0 ºC, utilizando un analizador ASAP modelo 2020 y porosimetro de Hg (modelo Autopore IV). Los ACMs se desgasificaron previamente durante 8 h a 150 ºC. Los parámetros texturales correspondientes se calcularon aplicando la ecuación BET y el método-t a partir de los datos de la isoterma de N_2 y mediante la ecuación de Dubinin-Radushkevich a partir de los datos de adsorción de CO_2. La distribución del tamaño de macroporos se calculó a partir de los datos de porosimetría de Hg.

A partir de las isotermas de adsorción-desorción de N_2 de los discos de ACM a -196 ºC, se observó que los ACMs obtenidos de la lignina Kraft y Alcell mostraron isotermas de tipo I característica de sólidos microporosos, donde casi todo el volumen de N_2 adsorbido tiene lugar a presiones relativas bajas. Concretamente, el monolito derivado de lignina Kraft presenta una meseta horizontal más pronunciada, comenzando con una presión relativa muy baja, lo que indica la presencia de una microporosidad más estrecha. Los monolitos obtenidos a partir de hueso de aceituna presentan una isoterma tipo IV con un aumento del volumen adsorbido en todo el rango de presiones relativas, en general, la

muestra obtenida a mayor relación de impregnación presenta un mayor desarrollo poroso, con estructuras micro y mesoporosas.

Por otro lado, el desarrollo de porosidad de los ACMs, a la misma relación de impregnación, sigue la secuencia: OS> AL> KL, probablemente debido a la presencia de celulosa en el hueso de aceituna que da lugar a un mayor desarrollo poroso.

Con respecto a la macroporosidad, las características observadas en las micrografías SEM fueron corroboradas en la distribución de tamaño de poro (PSD) obtenida a partir de la porosimetría de Hg. El monolito obtenido a partir de lignina Kraft exhibe la mayor contribución de macroporosidad. Por el contrario, la presencia de macroporos en los monolitos de hueso de aceituna es menor que en los monolitos derivados de lignina.

En el caso de la PSD obtenida por adsorción-desorción de N_2 a -196 ºC, se observó una amplia distribución del tamaño de los poros en todos los casos. Todos los ACMs presentan una banda principal centrada alrededor de 0,7 nm y un segundo pico que comprende tamaños de poro entre 1,4 y 2,0 nm. Los monolitos preparados a partir de lignina Kraft y Alcell muestran, ambos, una distribución bimodal en todo el rango de los microporos.

En el caso de los ACMs elaborados a partir de hueso de aceituna (OS1 y OS2) se observa una distribución de tamaño de poro más amplia, obteniendo mesoporos de hasta 4 nm. Este efecto es más notorio en la muestra OS2 debido a la mayor relación de impregnación, lo que produce un ensanchamiento de la porosidad.

Los monolitos exhibieron áreas superficiales aparentes (A_{BET}) entre 700 y 1500 m^2/g, lo que sugiere que los monolitos presentaban una estructura porosa bien desarrollada, además, el monolito OS2 es el que mostraba el área BET y el área externa (At) más alta (OS2= 1489 m^2/g > OS1= 1147 m^2/g > AL1= 1054 m^2/g > KL1= 682 m^2/g.

El análisis de la porosidad sugiere que la extrusión no modifica la estructura porosa del carbón activado, incluso en algunos casos se observó un ligero aumento de la superficie aparente, cuando se compararon con carbones activos granulares obtenidos a partir de los mismos precursores y en las mismas condiciones de temperatura y relación de impregnación.

La densidad real de los ACMs se midió con un picnómetro de helio utilizando un equipo AccuPyc II 1340. La evaluación de las propiedades mecánicas de los ACM (máxima resistencia a la compresión) se llevó a cabo mediante un ensayo de compresión, usando un analizador Deben Microtest, donde la velocidad de compresión fue de 0,003 mm/s.

Es importante señalar que el monolito obtenido a partir de lignina Kraft presenta una mayor densidad real, pero también muestra el mayor porcentaje de porosidad 64%. Un parámetro relevante en aplicaciones electroquímicas es la densidad aparente, que se puede calcular a partir de la porosidad y la densidad real. Los valores aquí obtenidos van desde 0,7 para KL1 a 1,4 g/cm3 para OS1, estos valores son considerablemente más altos que otros reportados en la literatura. En cuanto a la resistencia mecánica de los ACMs, los valores de resistencia a la compresión observados se encuentran en el mismo rango que los reportados para diferentes materias primas, siendo el valor más alto el obtenido por el monolito obtenido a partir de la lignina Alcell con 7.56 MPa.

La química superficial de los ACMs se analizó mediante desorción a temperatura programada (TPD) y espectroscopía fotoelectrónica de rayos X (XPS). Los perfiles de CO y CO_2 se obtuvieron en un reactor de lecho fijo de cuarzo colocado dentro de un horno eléctrico y se cuantificaron mediante analizadores de gases de infrarrojos no dispersivos (NDIR) (Siemens ULTRAMAT 22). Las muestras se calentaron desde temperatura ambiente hasta 930 ºC, a una velocidad de calentamiento de 10 ºC/min en un flujo de N_2. Los análisis XPS de las muestras se obtuvieron mediante un aparato “5700C model Physical”, con radiación de Mg Kα (1253,6 eV). Para el análisis de los picos XPS,

el máximo del pico del espectro del C1s se fijó en 284,5 eV y se utilizó como referencia para mover los otros picos.

Para todos los monolitos, las cantidades totales de CO liberadas fueron considerablemente mayores a las cantidades desorbidas de CO_2 durante los análisis de TPD, y que esta evolución tuvo lugar a temperaturas altas (mayores de 700 ºC), lo que sugería la presencia principal de grupos carbonilos, quinonas y grupos superficiales asociados al fósforo. Además, se encontró que las cantidades de CO desorbido fueron significativamente mayores para la muestra KL1 y muy similares para los monolitos de carbono AL1 y OS2. La concentración másica superficial de los ACMs fue determinada por XPS, los ACMs mostraron concentraciones de carbono en la superficie superiores al 78%, concentraciones de oxígeno de 7,8 a 18,8% y concentraciones de fósforo superiores al 2%, con el valor más alto encontrado para el monolito KL1. Analizando el espectro del fósforo se observó que el monolito KL1 es el que presentaba la mayor contribución de especies de fósforo más oxidadas (tipo -C-O-PO_3), mientras tanto, el monolito AL1 mostraba la mayor proporción de las especies de fósforo más reducidas (-C_3-PO).

Aplicaciones de los ACMs

Monolitos de carbón activado de residuos de biomasa lignocelulósica para aplicaciones electroquímicas

La caracterización electroquímica de los ACMs se realizó mediante técnicas de voltamperometría cíclica y carga-descarga galvanostática directamente con los electrodos de ACMs en ausencia de cualquier tipo de aglomerante y/o promotor de conductividad. Para ello se usó un analizador electroquímico modelo SP- 200 (Bio-Logic Int.) y una celda estándar de tres electrodos que consta de un alambre de platino como contra-electrodo, un electrodo de Ag/AgCl como electrodo de referencia y un electrodo de trabajo que contiene el ACM correspondiente con un espesor aproximado de 200 μm, previamente secado a 100ºC en una estufa de vacío. El colector consta de una malla de acero inoxidable. Los electrodos de trabajo y los contraelectrodos se colocaron cara a cara y se probaron en un electrolito 1 M H_2SO_4. Las muestras se caracterizaron mediante la técnica de voltamperometría cíclica a una velocidad de barrido de 1 mV s^{-1} y mediante la técnica de carga-descarga galvanostática (GCD) de 0 a 0,8 V vs Ag/AgCl/Cl-3M hasta densidades de corriente de 1000 mA/g. Las capacitancias de los experimentos de GCD (Cg^{GCD} y Cv^{GGD}) se calcularon a partir del perfil de descarga de GCD. Concretamente, las capacitancias específicas y volumétricas se

obtuvieron de las voltamperometrías cíclicas (CV), a 1mV/s, y de los ciclos de carga-descarga de corriente constante (GCD), a 50 mA /g.

El monolito de hueso de aceituna OS2 presentó la mayor capacitancia específica de todos los ACM, aproximadamente 217 F/g (capacitancia volumétrica de 205 F/cm^3), seguido de cerca del monolito KL1. Según el mecanismo de la doble capa, la capacitancia específica debería ser proporcional al área superficial aparente, sin embargo, la buena respuesta electroquímica del monolito KL1 sugería la presencia de pseudo-capacitancia debida a reacciones redox de los diferentes grupos oxigenados superficiales presentes en los monolitos (grupos quinonas y enlaces P=O presentes en los polifosfatos).

En cualquier caso, los valores de capacitancias específicas para los ACMs son comparables o incluso mejores que otros reportados en la literatura con porosidad similar, pero las capacitancias volumétricas de OS2 y AL1 son considerablemente más altas que los valores obtenidos en condiciones similares por otros autores. Además, la ventaja de estos materiales es el uso de un método de preparación simple para obtener electrodos de ACM a partir de precursores de residuos de biomasa.

Monolitos de carbono mesoporosos ácidos a partir de residuos de biomasa lignocelulósica para la deshidratación de metanol

La acidez de los ACMs fue determinada mediante la reacción de descomposición de Alcohol Isopropílico (IPA), donde en los sitios ácidos se lleva a cabo la deshidratación a propileno, y en los sitios básicos, la deshidrogenación a acetona. La descomposición del IPA se realizó en atmósfera inerte y a presión atmosférica en un microrreactor de lecho fijo de cuarzo de 6 mm de diámetro, que se colocó dentro de un horno vertical con control de temperatura. El IPA se alimentó al reactor mediante una bomba de jeringa (modelo Cole-Parmer® 74900-00-05, Vernon Hills, IL, EE. UU.), asegurando un flujo de IPA controlado constante, utilizando una presión parcial de IPA de 0.03 atm y un tiempo espacial de W/F_{0IPA} = 0,1 g s/µmol. Las concentraciones de reactivo y productos se analizaron mediante cromatografía de gases (micro-GC 490 equipado con un tamiz molecular PPQ, 5A, y una columna Wax, Agilent Technologies, Santa Clara, CA, USA).

En general, la conversión de IPA aumentó con la temperatura de reacción y el monolito OS2 mostró una actividad catalítica más alta que los otros ACMs a cualquier temperatura. El principal producto de reacción fue propileno derivado de la reacción de deshidratación. La selectividad al propileno fue muy alta en todas las temperaturas evaluadas. Solo se

observaron pequeñas cantidades de diisopropiléter a bajas temperaturas, mostrando una selectividad a propileno mayor al 90% para temperaturas superiores a 250 °C, para todos los ACMs. Los resultados sugirieron que los ACMs desarrollaron una cantidad relativamente grande de acidez superficial durante el procedimiento de preparación y, por lo tanto, no habría necesidad de tratamientos adicionales para aumentar la acidez de estos catalizadores.

A partir de estos datos, se obtuvieron los valores de la constante de velocidad aparente, k, utilizando valores de conversión inferiores al 20% y teniendo en cuenta una cinética global de primer orden. Los valores que se obtuvieron para las energías de activación aparentes fueron bastante similares, oscilando entre 100 y 130 kJ /mol y del mismo orden de magnitud que los publicados para diferentes catalizadores inorgánicos.

Los valores de los factores preexponenciales pueden proporcionar una estimación aproximada de la cantidad de sitios activos por unidad de superficie o unidad de masa de catalizador. A partir de los resultados obtenidos, se observó que el monolito KL1 era él que mostraba los valores más altos de energía de activación y factor preexponencial, lo que evidenciaba que el número de sitios activos estaba directamente

relacionado con la cantidad de grupos superficiales de fósforo presentes en los diferentes ACMs.

Descomposición de metanol

La descomposición del metanol se realizó en el mismo microrreactor utilizado para la prueba de descomposición de IPA. La reacción se llevó a cabo con 200 mg de ACM, en aire, a temperaturas entre 150 y 375 ° C. Todas las líneas se calentaron hasta 120 ° C para evitar cualquier condensación. La presión parcial de entrada de metanol fue de 0,03 atm y las presiones parciales del agua se variaron de 0 a 0,08 atm, con un tiempo espacial de 0,1 g s/µmol.

Las concentraciones de gas de salida se cuantificaron mediante cromatografía de gases (micro-GC 490 equipado con un tamiz molecular PPQ, 5A, y una columna Wax, Agilent Technologies, Santa Clara, CA, USA).

La conversión se definió como la relación entre la cantidad de metanol que se convirtió y la cantidad de metanol añadida al reactor. La selectividad (en % moles) se definió como la relación molar de un producto específico a la cantidad de metanol convertido. El balance de carbono se alcanzó con un error inferior al 3% en todos los casos.

Una vez que la acidez de los ACMs fue evidente, estos catalizadores se utilizaron para la reacción de deshidratación del metanol. Para ello se

seleccionó una temperatura de 375 °C como la temperatura de reacción máxima que pueden soportar los monolitos de carbono sin una significativa gasificación de la matriz carbonosa. La conversión más alta obtenida fue aproximadamente del 70% a 375 ° C, siendo OS2 el ACM más activo debido a su mayor valor de área superficial aparente, lo que compensa su contenido de P ligeramente menor. El resto de ACMs sigue la secuencia OS1> KL1> AL1.

El dimetiléter (DME) fue el principal producto de reacción. La selectividad a este producto fue superior al 90% para todos los ACMs hasta 350 °C. A 375 °C, la selectividad a DME disminuyó a alrededor del 85% debido a la aparición de CO_2 y, en menor medida CO, en la corriente de salida. La combustión de los ACMs fue considerable a temperaturas más altas y, por ello, no se evaluó la deshidratación del metanol a temperaturas mayores. Los complejos superficiales de fósforo del tipo C-O-P juegan un papel importante para una deshidratación de metanol eficiente y altamente selectiva a DME, debido a que poseen una acidez débil-moderada y proporcionan a la superficie del carbón de una alta resistencia a la oxidación. De hecho, estos sitios activos presentan una función redox, que evita (en presencia de aire) la desactivación del catalizador por deposición de coque debido a una (re) oxidación continua de las especies de P reducidas producidas durante la reacción de

deshidratación, y encima evitando una significativa gasificación del soporte carbonoso.

Estudio de estabilidad

Con el objetivo de estudiar la estabilidad con el monolito que presentó los mejores resultados de conversión y selectividad (monolito OS2), se llevó a cabo un experimento a largo plazo a dos temperaturas diferentes, a 300 y 350 °C, con una P_{MeOH} = 0,03 atm y W/F_{MeOH} = 0,1 g·s/µmol. Casi no se observó disminución del rendimiento a DME a 300 ° C durante más de 20 h de tiempo de reacción, lo que evidenció la alta estabilidad de este catalizador en estas condiciones de operación. A 350 °C, sí que se pudo observar una disminución gradual de la conversión de metanol, que estuvo principalmente relacionada con una desactivación progresiva del catalizador por deposición de coque. Sin embargo, es importante señalar que se han obtenido conversiones de metanol superiores al 45% durante más de 20 h, con selectividad hacia DME mayores al 85%.

Influencia del vapor de agua en la mezcla de reacción

La reacción de deshidratación del metanol a DME puede verse significativamente influenciada por la presencia de vapor de agua, que puede tener un efecto sobre el equilibrio de la reacción. Por ello, también se analizó la influencia de la presencia de agua en la conversión de

metanol para el monolito que mostraba la mayor actividad, OS2, a diferentes presiones parciales de agua, a 300 y 350ºC para una presión parcial de metanol de P_{MeOH} = 0,03 atm, y un tiempo espacial, W/F_{MeOH} = 0,1 g s/µmol.

Las conversiones de metanol disminuyeron significativamente en presencia de agua, en comparación con las conversiones de equilibrio, lo que se debió a la adsorción competitiva del agua con el metanol por los sitios ácidos del catalizador. Específicamente, la conversión de metanol se redujo a la mitad en presencia de 0.08 atm de vapor de agua, a 350 ° C, mientras que se observó una disminución de casi el 70% a 300 ° C, lo que indicó que la influencia del agua fue menos pronunciada con el aumento de temperatura de reacción. Este hecho probablemente se debió a que la entalpía de adsorción del agua era ligeramente superior a la del metanol. La formación de DME también disminuyó del 99 al 86% en presencia de 0.08 atm de agua, a 300 ° C. Al comparar estos resultados con un carbón activo en polvo, obtenido a las mismas condiciones de relación de impregnación y temperatura de activación, se observó una disminución menos pronunciada que la observada para el monolito OS2, a pesar de que tanto el carbón activado en polvo como el monolito (OS2) presentan contenidos de P muy similares, por XPS. Sin embargo, las condiciones experimentales para estos dos casos fueron ligeramente

diferentes, ya que la concentración inicial de metanol fue menor para el caso del carbón activado en polvo, lo que supondría una menor formación de agua por la reacción y, por tanto, una menor adsorción competitiva entre el metanol y el vapor de agua.

Estudio cinético

Los datos de conversión de metanol en estado estacionario que se obtuvieron a diferentes temperaturas se ajustaron utilizando varios modelos cinéticos para un reactor integral. La ecuación de balance de materia del reactor se integró numéricamente para calcular la conversión de metanol.

Para ello, se ha supuesto que la deshidratación del metanol fue la reacción predominante, puesto que la selectividad hacia el dimetiléter fue superior al 90% en la mayoría de los experimentos. Además, se tuvo en cuenta la adsorción competitiva de agua en los sitios activos, que es responsable de la disminución de la actividad catalítica. El oxígeno no se incluyó en la ruta de reacción principal y su función se atribuyó a la oxidación de los intermedios que proporcionarían la desactivación del catalizador mediante la formación de hidrocarburos ligeros y coque.

A partir de estas consideraciones, se propusieron tres modelos cinéticos para describir la velocidad de descomposición del metanol: (i) Pseudo-segundo orden (SO) con respecto a la concentración de metanol, (ii)

Mecanismo Langmuir-Hinshelwood (LH), y (iii) Mecanismo Eley-Rideal (ER). Los mecanismos LH y ER también incluían la adsorción competitiva de agua.

Los parámetros cinéticos y de adsorción relacionados de las ecuaciones de Arrhenius y Van't Hoff se optimizaron minimizando la función objetivo (OF). La optimización se realizó utilizando un método de búsqueda simplex.

Los resultados de la optimización revelaron que el modelo de segundo orden (SO) no podía reproducir adecuadamente los datos experimentales. El modelo más probable parece ser el LH, que es para el que se obtuvo el error más bajo, aunque serían necesarios más experimentos a presiones de metanol más altas para confirmar este hallazgo.

El modelo LH también era capaz de describir bien la influenciade la presencia de agua en la alimentación del reactor sobre la conversión de metanol. En este sentido, el mecanismo de LH con adsorción de agua competitiva proporciona las mejores predicciones del modelo para la conversión de metanol con el monolito OS2, cuando se introdujeron diferentes cantidades de vapor a la entrada del reactor a 300 y 350 ° C.

Las energías de activación que se obtuvieron se encuentran dentro del estándar de las encontradas previamente para otros catalizadores de

carbón activado utilizados para la deshidratación de metanol. El monolito más activo, OS2, mostró el valor de energía de activación más bajo. Además, la evaluación de la constante cinética y de adsorción a 300 ° C reveló que el valor de la constante cinética siguió el orden OS1> AL1> OS2 > KL1, mientras que la constante de adsorción mostró una tendencia bastante diferente, OS2> KL1 > OS1> AL1. La combinación de ambos valores constantes puede explicar la mayor conversión de metanol que se logró a menores temperaturas para los monolitos OS1 y OS2. Por otro lado, la menor afinidad de la superficie de OS1 por el metanol explicaría por qué el monolito OS2 supera al OS1, a medida que aumenta la temperatura de reacción. La evaluación del valor de la constante de adsorción del agua K_{H2O} a 300 ° C (15,8 atm^{-1}) reveló que la afinidad de la superficie del monolito OS2 hacia el agua era mayor que hacia el metanol en esas condiciones. Por lo tanto, la adición de agua al gas de entrada podría desplazar efectivamente al metanol de los sitios de adsorción cuando su presión fuera lo suficientemente alta, un hecho que podría estar detrás de la caída de actividad que se observó para el monolito OS2, en presencia de vapor de agua.

Conclusiones generales

En esta tesis se han preparado monolitos cilíndricos de carbón activado (ACM) mediante activación química de diferentes residuos de biomasa lignocelulósica (hueso de aceituna, Alcell y lignina kraft) con ácido fosfórico a diferentes relaciones de impregnación. La extrusión de la mezcla adecuada, sin ningún tipo de aglomerante, se realizó en una extrusora diseñada por nuestro grupo de investigación con diferentes elementos de matriz. Con esta extrusora es posible obtener discos y monolitos de 25 y 120 canales/cm^2.

El precursor con un tamaño de partícula adecuado se mezcla con una disolución de H_3PO_4 hasta obtener las propiedades reológicas adecuadas para ser extruida. El monolito resultante se activa a 700 ºC y luego se lava con agua destilada hasta pH constante.

En el caso de los precursores de lignina, se realizó el proceso de estabilización para minimizar los problemas de plasticidad e hinchamiento. La mitad de la muestra impregnada se trata a 250 ºC en aire y se mezcla con el resto de la muestra impregnada antes de la extrusión. Utilizando hueso de aceituna como precursor, se obtuvo un monolito de carbón microporoso activado con una superficie aparente de unos 1500 m^2/g, con un volumen de microporos de 0,538 cm^3/g a 700 ºC con una relación de impregnación de 2. La densidad aparente de los

monolitos también es muy alta (~1,1 g/cm^3 para ACM de lignina Alcell), con una resistencia a la compresión de 7,6 MPa. Esta alta densidad abre todas las posibilidades a diferentes aplicaciones.

La caracterización electroquímica se realizó mediante técnicas de voltamperometría cíclica y carga-descarga galvanostática con electrodos de ACM en ausencia de cualquier tipo de ligante y promotor de conductividad. El monolito de hueso de aceituna presenta la mayor capacidad específica de todos los ACM, aproximadamente 217 F/g. Este valor es superior a otros reportados en la literatura para carbones activados obtenidos a partir de precursores lignocelulósicos.

Los monolitos de carbón activado preparados mediante activación química de diferentes residuos de biomasa lignocelulósica se utilizaron también como catalizadores para la reacción de deshidratación del alcohol. La conversión más alta para la descomposición del IPA se obtuvo para el ACM de hueso de aceituna OS2. La selectividad hacia propileno fue bastante alta en todas las temperaturas evaluadas, siendo superior al 90% a partir de 250 °C, para todos los ACMs. Los valores de las energías aparentes de activación obtenidas (suponiendo una cinética de primer orden) fueron bastante similares, oscilando entre 100 y 130 KJ/mol.

La reacción de descomposición del metanol también se analizó en atmósfera de aire. La conversión más alta obtenida, sin una gasificación significativa de la matriz carbonosa, fue de aproximadamente 70% a 375 °C, siendo el catalizador OS2, el más activo, seguido por KL1 y AL1.

Por otro lado, también se evaluaron varios modelos cinéticos para predecir las conversiones de metanol, teniendo también en cuenta la influencia competitiva del agua. El mecanismo de Langmuir-Hinshelwood, cuyo paso limitante de la velocidad fue la reacción superficial entre dos moléculas de metanol adsorbidas, representó muy bien los datos experimentales en las condiciones estudiadas. Se obtuvo un valor de energía de activación de 92 kJ/mol para la reacción de deshidratación de metanol y entalpías de adsorción para metanol y agua de −12 y −35 kJ/mol, respectivamente.